https://doi.org/10.1016/j.buildenv.2020.107195

Effects of height-asymmetric street canyon configurations on outdoor air temperature and air quality

Zhengtong Li [a], Hao Zhang [a], Chih-Yung Wen [a], An-Shik Yang [b,*] , Yu-Hsuan Juan [b]

[a] Department of Mechanical Engineering and Interdisciplinary Division of Aeronautical and Aviation Engineering, The Hong Kong Polytechnic University, Kowloon, Hong Kong

[b] Department of Energy and Refrigerating Air-Conditioning Engineering, National Taipei University of Technology, Taipei 106, Taiwan, ROC

* corresponding author

Abstract:

This paper investigates the effects of height-asymmetric street canyon configurations on air temperature and air quality at the pedestrian level using the ANSYS Fluent® software. The study concerns the situation with a subtropical city where there is a predominant wind direction (as is the case in, e.g., Hong Kong) and where the direction of that wind is perpendicular to the street canyon, since this is the worst-case from air pollution and overheating point of view. In particular, this North-South oriented street has been studied with the realistic solar irradiance at two different sun directions, corresponding to morning (08:00) and afternoon (16:00) hours, respectively. Two step-up and two step-down North-South oriented street canyons are considered under two different incoming wind speeds (high and low). The corresponding ratios of upwind and downwind building heights are= 1/3, 2/3 and 3/1, 3/2, respectively.

The results demonstrated that for the step-up canyon, a higher upwind building was found to produce a hotter air temperature only at a low wind speed and polluted more severely at both high and low wind speeds, compared with its lower upwind building counterpart. In contrast, for the step-down canyon, a higher downwind building was found to produce cooler air temperatures at both high and low wind speeds and accumulated more pollutants only at a low wind speed, compared with its lower downwind building counterpart. On the other hand, at the high wind speed, both air quality and thermal environment were better in the step-up canyon than in the step-down canyon. However, at the low wind speed, the air quality was higher in the step-down canyon than the step-up canyon, while the step-up canyon still provided better thermal environment than the step-down canyon. Moreover, a Richardson number (Ri) for the asymmetric street canyons is defined for the evaluation of the buoyancy force versus the inertial force. When $|Ri| > 20$, the flow field was mainly dominated by natural convection, and an increase of $|Ri|$ resulted in an increase in the air temperature and a decrease in the pollutant concentration. In contrast, when $|Ri| < 20$, the flow field was dominated by forced convection, and the variation of $|Ri|$ had an insignificant influence on air quality and air temperature. The simulated pollutant concentration and thermal environment results were further processed to obtain optimization guidelines for a north-south asymmetric canyon in the city centers of Hong Kong via the application of multivariate regression analysis with a group of dimensionless parameters. These guidelines will facilitate the renewal of north-south asymmetric street canyons while enhancing air quality and lowering air temperature by serving as a reference for architects.

Keywords: Asymmetric street canyon; outdoor thermal comfort; air quality; realistic solar radiation; computational fluid dynamics

1. Introduction

Recently, urban renewal has become a critical issue throughout the transitional periods of large- and medium-sized cities all over the world [1–4]. By replacing old and low constructions with high-rise buildings, the resulting rise of the urban air temperature and deterioration of the urban air quality can be expected to affect humans if no careful urban planning is conducted for these high-rise buildings [5–10]. The rational utilization of urban renewal and the development of more comfortable urban spaces have become significant research areas due to health concerns [11–15]. Thus, the objective of this study is to propose a practicable asymmetric street canyon model for the simultaneous realization of higher air quality and lower air temperature.

During the urban renewal process, there are always variations in terms of building height; thus, urban structures often present irregular building patterns in urban canyons [16]. However, the effect of the uneven building layout is often neglected. According to Gu et al. [17], studies that are based on uniform street canyon models cannot identify the flow structure in non-uniform street canyons. Consequently, investigation of the effects of asymmetric urban arrangement will facilitate our understanding of pollutant and heat dispersion in actual urban areas and enable us to create better outdoor environments at the phase of urban renewal.

A few studies have focused on asymmetrical urban structures for the enhancement of ventilation or the reduction of thermal stress, which are summarized in Table 1. The following general observations are made:

(i) Without considering solar radiation

Xie et al.[18], Yang et al.[19], and Hao et al.[20] reported that the flow patterns are strongly related to the asymmetry aspect ratio (the ratio between the leeward and windward building heights) for 2D models. The change in flow patterns could further affect the dilution potential of in-canyon traffic-induced pollutants. Hence, Assimakopoulos et al. [21] and So et al.[22] compared the pollutant concentration in step-up and step-down street canyons. It is found that pollutant levels are raised in a step-down street canyon (higher buildings upstream) but reduced in a step-up street canyon (higher buildings downstream) in two-dimensional (2D) models. Moreover, the influence of asymmetric aspect ratios (upwind building height to downwind building height) on the pollutant dispersion process was investigated by Yang et al. [19] and Hao et al. [20]. Yang et al. [19] showed that asymmetric aspect ratios from 2/7 to 7/2 are favorable for the realization of higher air quality. According to Hao et al. [20], an increase of the height of a windward building of the step-up notch hinders the diffusion of pollutants. Furthermore, the ventilation potential and flow characteristics of the 3D asymmetric street canyons were discussed. Gu et al. [17] and Miao et al. [23] determined that an asymmetric configuration (step-up or step-down street canyon) could provide better ventilation because the lower parts of the street canyon are occupied by the divergent flows of the strong downdraft flow. Park et al. [24] investigated the flow characteristic around step-up street canyons with a various building aspect ratio (building length-width ratio and asymmetric aspect ratio). With an increase in the building length-width ratio, the in-canyon flows can undergo development and mature stages. Besides, a deep asymmetric aspect ratio causes a strong downward airflow in the center of the street canyon but a weak outward airflow near the ground, particularly at the mature stage. Similarly, Addepalli and Pardyjak [25,26] found that the topological flow features around the asymmetric street canyon are largely sensitive to the ratio of upwind and downwind building heights.

(ii) With the consideration of solar radiation

Xie et al. [27] investigated the impact of solar radiation on pollutant dispersion in two asymmetric 2D street canyons. The results demonstrated that the pollutant concentration increases when the windward side of the step-up notch or the leeward side of the step-down notch is heated. Qaid and Qssen [28] reported that asymmetrical streets outperform shallow symmetry streets in enhancing wind flow and blocking solar radiation to provide superior thermal comfort. Similarly, Rodríguez-Algeciras et al.[29] showed that high facades that are located on the east-facing side of north-south (N-S) streets reduce the thermal burden effectively.

Although previous studies have provided many findings regarding the design of uneven building layouts for the realization of higher air quality or a better thermal environment, they are still not sufficient for the formulation of guidelines for practical urban planning to reduce thermal stress and improve air quality simultaneously. First, the effect of solar radiation was neglected by most previous studies on asymmetric street canyons. In practice, the thermally induced flow is typically combined with the mechanically induced flow, which significantly affects the flow field and dispersion of pollutants and heat[30–33]. Second, most of the papers focused on either air temperature or air quality only when solar radiation was considered; only very limited studies addressed the increasingly severe issues of air temperature and air quality simultaneously[34]. Finally, the effect of the incoming wind speed should be considered to cover different atmospheric wind conditions with the consideration of solar radiation [35,36]. Notably, the step-up canyon is easily switched to the step-down canyon with a significant variation of prevailing wind direction. It, then, makes little sense to study the difference of step-up and step-down canyons. However, for some cities, there could be a very clear prevailing wind direction. In Hong Kong, the east wind is quite prominent for the whole year [37], as shown in Table A.1. Accordingly, it is important to differentiate the step-up street canyon from the step-down canyon.

On the basis of this background, the objectives of this study are 1) to simulate emissions from vehicle exhausts and the thermal environment under the effects of solar radiation; 2) to evaluate the effects of realistic solar radiation and the corresponding shading effects for various configurations (the step-up and step-down street canyons) under two different incoming wind conditions; and 3) to identify critical building configurations that would enhance ventilation and improve the thermal environment for some tropical or subtropical cities suffering strong urban heat island effects and poor air quality (e.g. Hong Kong, Singapore and Kuala Lumpur)[38].

Table 1 Overview of Computational Fluid Dynamic (CFD) studies on the urban microclimate problem (air quality and air temperature) in asymmetric street canyons

Study	Ref.	Solar radiation	Focus	Sensitivity analysis	Street configuration	Main conclusion
Assimakopoulos et al. 2003	[21]	No	AQ	a	2D	Pollutant level is increased in the step-down notch but decreased in the step-up notch
Xie et al. 2005	[18]	Yes	AQ	a, c	2D	Pollutant concentration is increased when the windward side of the step-up notch or the leeward side of the step-down notch is heated
So et al. 2005	[22]	No	AQ	a	2D	The downstream buildings of the step-down notch could hinder the dilution of pollutant compared to those of the step-up notch.
Xie et al. 2006	[27]	No	AQ	a	2D	Three regimes were defined according to the street width and the asymmetric aspect ratio
Gu et al. 2011	[17]	No	AQ	a	3D	Uneven building layouts can improve the dispersion of pollutants
Miao et al.	[23]	No	AQ	a	3D	Asymmetric configuration (step-up

2014						or step-down street canyon) could provide better ventilation
Qaid and Qssen 2015	[28]	Yes	AT	a, b	3D	Asymmetrical streets outperform low-symmetry streets in enhancing wind flow and blocking solar radiation
Yang et al. 2017	[19]	No	AQ	a	3D	Asymmetric aspect ratios from 2/7 to 7/2 are favorable for realizing higher air quality
Rodríguez-Algeciras et al. 2018	[29]	Yes	AT	a, c	3D	High facades that are located on the east-facing side of N-S streets effectively reduce thermal stress
Hao et al. 2019	[20]	No	AQ	a	2D	Increase of the heights of the windward buildings of a step-up notch hinders the diffusion of pollutants. The canyon with asymmetric aspect ratios =6/5 has the lowest pollutant concentration.

Notes: AQ= Air quality, AT= Air temperature. The "Sensitivity analysis" entry refers to aspects that have been investigated in each study: (a) the street canyon geometry (asymmetric *H*/*W* aspect ratio and street width), (b) the ambient wind parameters (wind velocity and direction), and (c) the distribution and strength of the surface thermal flux (solar position, temperature difference between wall and air, and shading effect).

2. Methodology

2.1 CFD numerical model

2.1.1 Model description and simulation setup

Two urban renewal processes that are associated with asymmetric street canyons are investigated in this study: 1) The high building that is present, the low building that will be rebuilt, and the height to which this building should be rebuilt to realize our objectives will be explored. 2) One of the buildings of a symmetric street canyon will be replaced by a higher building, and the side of the street on which it should be rebuilt will be investigated.

A step-up (or step-down) street canyon, as illustrated in Fig. 1(a), is defined as a street canyon in which the upstream building height (H_1) is smaller (or larger) than the downstream building height (H_2) with a fixed street width of W = 20 m, a building width of W_b = 20 m, and a building length of L = 100 m. As illustrated in Fig. 1(b), four configurations with various asymmetric aspect ratios, which are defined as H_1/ H_2, were considered for these two urban renewal processes. In June, the wind speed of

Hong Kong occurs most frequently at 3 m/s from the east (measured at the height of 32 m above sea level)[37]. Considering the perpendicular wind generally yields a worse air quality within the street canyon[39]. The street orientation was set as a North-South direction (Fig.1 (a)), accordingly.

The theoretical model, which was formulated in ANSYS/Fluent® CFD software (Release 15.0), was used to simulate the flow of ambient wind over an asymmetric street canyon (step-up or step-down) under the effect of realistic solar heating for the evaluation of air temperature and air quality at the pedestrian level (1.5m above the ground). According to the practice guidelines by Tominaga et al.[40], the dimensions of the computational domain are based on the parameter H_{max} (= max(H_1, H_2)= 60 m) as follows: the axial distance between the velocity inlet and the windward face of the upstream building is 5 H_{max}, the transverse distances between the sidewalls of the buildings and the symmetric boundaries on both ends are all 5 H_{max}, and the outlet boundary is 15 H_{max} from the leeward faces of the downstream buildings, as specified in Fig. 1 (a).

In addition to simulations for identifying the effect of the aspect ratio, simulations were conducted for steady-state weather conditions at LSTs (local solar times) of 8 am (0800 LST) and 16 pm (1600 LST) on a clear summer day in Hong Kong (latitude: 22°18' N, longitude: 114°10' E; date: June 15) with two different inlet temperatures (27.3 °C for 8 am and 29.1 °C for 16 pm). As shown in Fig. 1 (a), the sun rises in the east in the morning (8 am) and sets in the west in the afternoon (16 pm). Additionally, two different incoming airflow conditions (0.5 m/s for low wind speed and 3 m/s high wind speed) are considered for various Richardson numbers. The profiles of the neutral ABL velocity (U_{ABL}), turbulent kinetic energy (k), and turbulence dissipation rate (ε) were resolved as[41]

$$U_{ABL} = \frac{u^*_{ABL}}{K} \ln(\frac{z + z_0}{z_0}) , \tag{1}$$

$$k = \frac{(u_{ABL}^*)^2}{\sqrt{C_\mu}} \quad , \qquad (2)$$

$$\varepsilon = \frac{(u_{ABL}^*)^3}{K(z + z_0)} \quad , \qquad (3)$$

where u_{ABL}^* is the ABL friction velocity, which can be calculated from the reference wind speed of U_{ref}=0.5 m/s (low wind speed) or 3 m/s (high wind speed) at a reference height h (32 m) using Eq. (4):

$$u_{ABL}^* = \frac{KU_{ref}}{\ln(\frac{h + z_0}{z_0})} \quad . \qquad (4)$$

In Eq. (4), K and z_0 are the von Karman's constant (≈ 0.4) and the aerodynamic roughness (=2 m) for city centers[42], respectively.

To accurately resolve the surface temperatures of buildings, the radiative heat fluxes that result from the significant solar radiation effect must be considered. With the inputs of the specific time and the global location, the accurate position of the sun can be calculated by the Solar Calculator dialog box of ANSYS Fluent®, and its Ray-Tracing model can provide the incident radiation on those exposed surfaces. Thus, the direct solar radiation was added into the energy equation as a source term Q_T. In other words, the thermal load resulted from solar radiation will be applied as a boundary condition. In addition, the discrete ordinate (DO) radiation model is applied to evaluate the radiant heat fluxes between the surfaces [43,44]. The spectral optical and thermophysical properties of the involved materials are summarized in Table A.2. The heat transfer coefficients (h_c) of the building faces and ground are calculated via the following empirical correlation [45]:

$$h_c = 5.7 + 3.8V_{air} \quad , \qquad (5)$$

where V_{air} is the average airflow velocity in the axial direction of the canyon (within the asymmetric canyons, blue regions in Figure A.1).

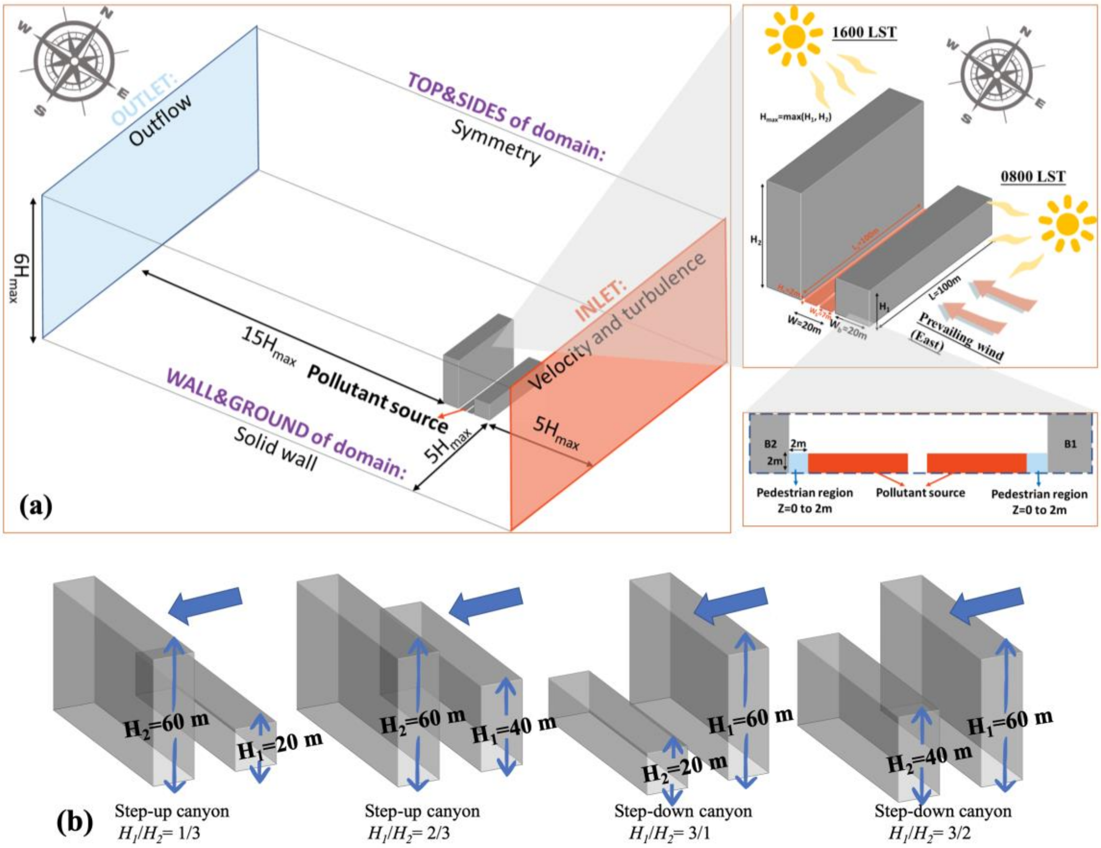

Fig. 1 (a) The geometric model and boundary condition and (b) various asymmetric street canyon configurations

2.1.2 Governing equation and turbulence model

The CFD simulations were conducted by the ANSYS Fluent® 15.0 [46] software to resolve the air velocity, temperature, and pollutant concentration fields. The analyses were based on the steady-state 3D RANS conservation equations of mass, momentum, and energy for the incompressible turbulent flow. The governing equations are as follows:

Continuity equation:

$$\frac{\partial u_i}{\partial x_i} = 0\,. \tag{6}$$

Momentum equation:

$$\frac{\partial \rho u_i u_j}{\partial x_j} = -\frac{\partial p}{\partial x_i} + \frac{\partial}{\partial x_j}\left[(\mu + \mu_t)\left(\frac{\partial u_i}{\partial x_j} + \frac{\partial u_j}{\partial x_i}\right)\right] + \rho_{ref}\, g_i \beta\left(T - T_{ref}\right). \tag{7}$$

Energy equation:

$$\frac{\partial u_i T}{\partial x_i} + \frac{\partial}{\partial x_i}(\alpha_T \frac{\partial T}{\partial x_i}) = Q_T \ , \tag{8}$$

where the term u_i denotes the i-axis component of the air velocity; p, ρ, T, μ, μ_t, g_i, and α_T represent the pressure, density, temperature, dynamic viscosity, turbulent viscosity, gravity acceleration and thermal diffusivity, respectively; and Q_T denotes the heat flux that is caused by solar radiation. To model the buoyancy-driven flow, we adopted the Boussinesq approximation, namely, $\rho = \rho_{ref}\,\beta(T\text{-}T_{ref})$, in Eq. (7), where β, T_{ref}, and ρ_{ref} are the thermal expansion coefficient, reference temperature, and reference density, respectively. This study treats the density as a constant value in all the equations, except for the buoyancy term in the momentum equation.

The species transport equation was solved to probe the pollutant dispersion in an urban environment as follows:

$$\frac{\partial u_i Y}{\partial x_i} - \frac{\partial}{\partial x_i}\left[\left(D + D_t\right)\frac{\partial Y}{\partial x_i}\right] = S \ , \tag{9}$$

where D and D_t (= ν_t/S_{ct}) denote the molecular and turbulent diffusion coefficients, respectively, of the pollutant. Here, ν_t is the turbulent viscosity and S_{ct} is the turbulent Schmidt number, which is set as 0.4 to account for the underestimation of the turbulent mass diffusion from the RANS models [47]. Y is the mass fraction of the pollutant. Herein, CO was used as a pollutant representative. To calculate the CO concentration, two uniform volume sources (width W_p = 7 m and length L_p = 100 m) of CO were specified near the ground with a depth of z = 0-2 m to represent traffic lanes on both sides, as shown in Fig. 1(a). The constant emission rate per hour and unit street length (36.1 g/h/m, i.e., total mass release rate of $L_p \times 1.0 \times 10^{-5}$ kg/s) is adopted for each CO source with reference to Ng and Chau [48]. Considering the type and number of vehicles passing by a realistic street per hour in Mongkok, Hong Kong, Ng and Chau [48] summarized the pollutant release rate above.

The steady RANS turbulence model was applied to evaluate the wind and thermal environments and the pollutant dispersion. The RNG k-ε model, which was developed by Yakhot and Orszag [49], has been demonstrated to be capable of simulating a wide range of turbulent flow phenomena for effectively characterizing the airflow and pollutant transport in street canyons under the thermal buoyancy force effects [50]. The conservation equations of the RNG k-ε turbulence model for the turbulence kinetic energy (k) and dissipation rate (ε) are as follows:

$$\frac{\partial \rho k u_i}{\partial x_i} = \frac{\partial}{\partial x_i}\left[(\mu + \frac{\mu_t}{\sigma_k})\frac{\partial k}{\partial x_i}\right] + P_k + G_b - \varepsilon \,, \tag{10}$$

$$\frac{\partial \rho \varepsilon u_i}{\partial x_i} = \frac{\partial}{\partial x_i}\left[(\mu + \frac{\mu_t}{\sigma_\varepsilon})\frac{\partial k}{\partial x_i}\right] + C_{\varepsilon 1}\frac{\varepsilon}{k}(P_k + C_{\varepsilon 3}G_b) - C_{\varepsilon 2}\frac{\varepsilon^2}{k} \,, \tag{11}$$

where $\mu_t = C_\mu \rho k^2/\varepsilon$. The values of the constants C_μ, σ_k, σ_ε, $C_{\varepsilon 1}$, and $C_{\varepsilon 2}$ are 0.0845, 0.7194, 0.7194, 1.42 and 1.68, respectively. The factor $C_{\varepsilon 3} = \tanh\left|\frac{v}{u}\right|$, where v and u are the velocity components of the flow that are parallel and perpendicular, respectively, to the gravitational vector. The production terms of the turbulent kinetic energy that is due to buoyancy (G_b) and shear (P_k) can be expressed as follows:

$$G_b = \beta \frac{\mu_t}{\Pr_t}\frac{\partial T}{\partial x_i} g_i \,, \tag{12}$$

$$P_k = \nu_t \left(\frac{\partial u_i}{\partial x_j} + \frac{\partial u_j}{\partial x_i}\right)\frac{\partial u_i}{\partial x_j} \,. \tag{13}$$

The standard wall functions by Launder and Spalding [51] with and without roughness modification by Cebeci and Bradshaw [52] were applied at the ground surface and the building surface, respectively. Herein, the sand grain roughness height k_s is calculated by the roughness constant C_s (=0.5) and the aerodynamic roughness z_0 (=2 m) in Eq. (14)[42].

$$k_s = \frac{9.793 z_0}{C_s} \,. \tag{14}$$

2.1.3 Numerical method

The presented governing equations were discretized via the finite volume scheme in a commercial software, namely, ANSYS Fluent®. This study utilized the pressure-linked equations-consistent (SIMPLEC) numerical method for the pressure-velocity coupling. The second-order upwind scheme was used to discretize both the convective terms and the diffusion terms. A double-precision solver was also selected for CFD calculations. The convergence criterion of the normalized residual errors of the energy equation was set to 10^{-9}, whereas the convergence criterion of the remaining equations was set to 10^{-6}.

2.1.4 Mesh description and mesh-independent validation

Prior to conducting CFD simulations, a mesh-independent test was conducted over three mesh resolutions (from coarse to fine). The grid information of these three grids on the horizontal section (*x*-*y* section) and vertical section (*x*-*z* section) across the tested street canyon are illustrated in Fig. 2 (a). To ensure the high quality of the computational mesh system, the computational domain was constructed using structured hexahedral cells. A grid expansion ratio of 1.05 in conjunction with the bi-geometric mesh law was set in both the vertical and horizontal directions in street canyons. Considering the relatively large gradients of the velocity and temperature near the ground and building surfaces, the finest grids around these two types of walls were deployed. Because the evaluation height should be located at the third or higher grid from the ground [46], the minimum sizes for the coarse grid, the medium grid, and the fine grid were set to be 0.5m, 0.4m, and 0.3m, respectively. In this way, all these three grids have an adequate resolution (at least three cells from the ground) for resolving the airflow and the distributions of temperature and pollutants at the pedestrian level, which is 1.5m above the ground. The total cell numbers for the coarse grid, the medium grid, and the fine grid are 0.5 million, 3.5 million and 12.3 million, respectively. Therefore, the ratio of two consecutive cell numbers for grid refinement in the mesh independent study can be at least 3.4[40]. Notably, the grid was refined at a factor of 1.5 in each direction at least. Further, three types of meshes were tested for the canyon (H_1= H_2= 20 m) under the same environmental conditions (0800 LST, U_{ref}= 3 m/s and T_{in} = 27.3 °C). According to Table 2, the comparisons of average wind speed, air temperature, and pollutant concentration at the pedestrian level show that the corresponding mean deviations between the fine grid and medium grid are less than 4%, indicating that the fine grid and medium grid yield considerably close results. In contrast, the mean deviation between the predictions of average wind speed and pollutant concentration by the medium grid and those by the coarse grid are even more than 34%. Accordingly, the medium grid (with a total cell number of 3.5 million), as shown in Fig.2 (b), was considered adequate and adapted to perform further numerical analysis. Besides, the average of *y*+ values on building surfaces for the medium grid under both high and low wind speed are less than the upper bound of *y*+ (500) for standard wall function recommended by An et al.[53].

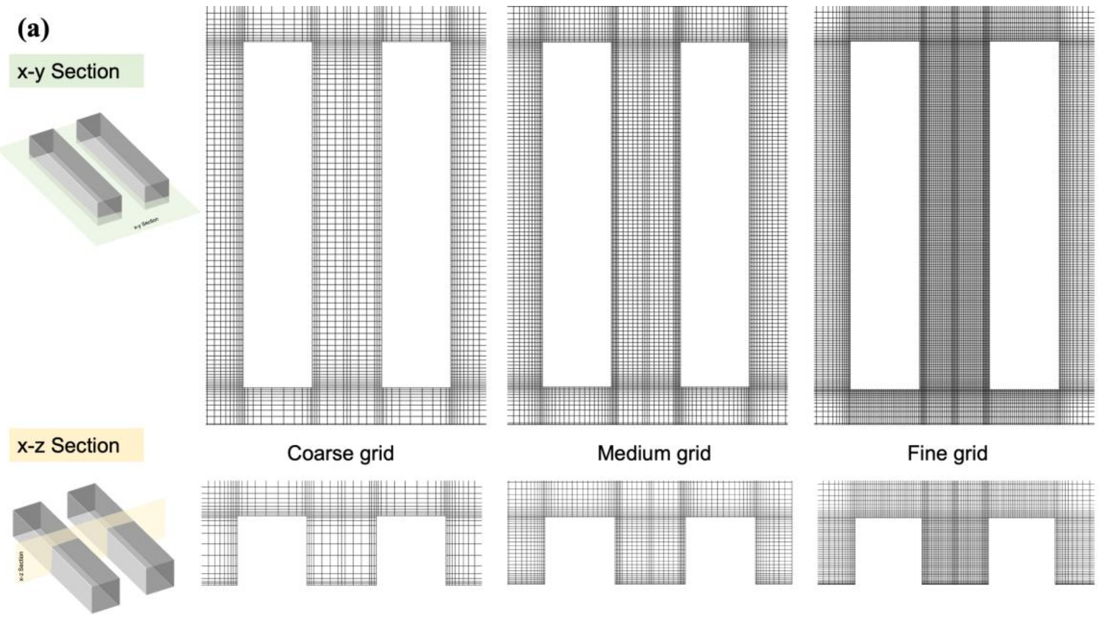

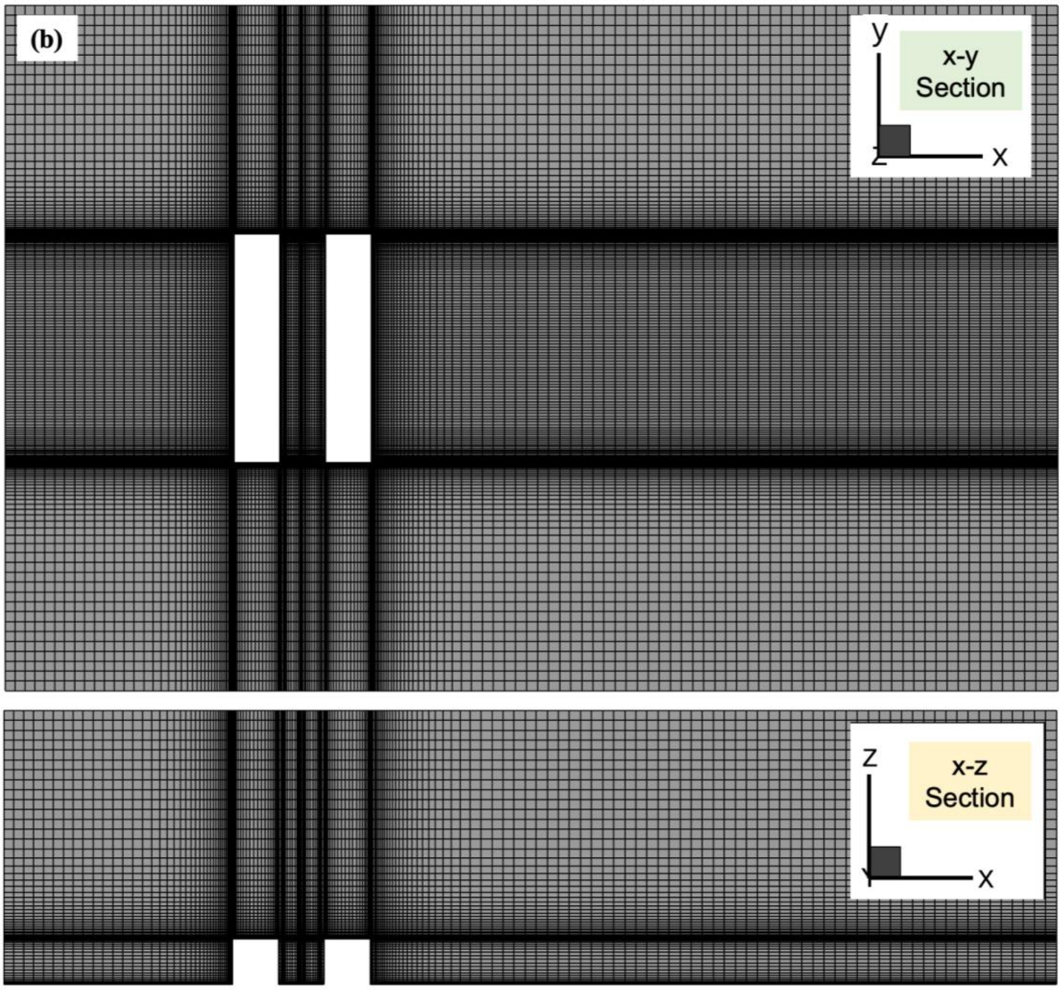

Fig.2 (a) Detailed information across the tested street canyon for all three mesh independence test cases and (b) Grid distributions of the geometric model : $H_1 = H_2 = 20$ m with the medium grid.

Table 2 Mesh independence study (0800 LST, $U_{ref} = 3$ m/s and $T_{in} = 27.3$ °C).

Cell numbers	First-layer thickness (m)	Maximum element size (m)	Average wind velocity at pedestrian level (m/s)	Average CO concentration at pedestrian level (mg/m^3)	Average air temperature at the pedestrian level (°C)
0.5 million	0.5	5	0.832	3.156	28.197
3.5 million	0.4	4	0.585	4.242	28.612
12.3 million	0.3	3	0.562	4.309	28.731

2.2 Richardson number in the asymmetric street canyons

Typically, the bulk Richardson number, Ri, is used to represent the atmospheric stability in the vertical direction[54]. Ri can be used to determine whether the induced flow field is dominated by the thermal or mechanical effect[55]. Herein, Ri of an asymmetric street canyon is defined as the ratio of the characteristic buoyancy force to the inertial force that is experienced by a fluid element, in consideration of the distribution of the wall temperature:

$$Ri = \frac{g\frac{H_1 + H_2}{2}(T_{in} - \frac{T_L + T_W}{2})}{U_{ref}{}^2 T_{in}} \quad (15).$$

In Eq. (15), T_W and T_L are the averaged surface temperatures on the windward and leeward surfaces, respectively, and U_{ref} is the volume-average wind speed within the asymmetric canyons (blue regions in Figure A.1). The reference height was $(H_1+H_2)/2$. T_{in} was the inlet air temperature (27.3 °C for 0800 LST and 29.1 °C for 1600 LST). If $|Ri|$ approaches ∞, the airflow within the street canyon that is induced by the mechanical effect can be ignored [27,55].

3. Results and discussion

3.1 Validation

3.1.1 Validation study of isothermal airflow in asymmetric street canyons

The current computational model for replicating the isothermal airflow within an asymmetric street canyon was validated against the wind tunnel measurements conducted by Addepalli and Pardyjak [26]. In the wind tunnel experiment, the flow features over a group of step-up street canyons were collected under the isothermal condition in a 7.9 m long boundary layer wind tunnel with a 0.91×0.61 m cross-section, as shown in Fig. 3(a). To validate the predicted flow structure and airflow speed, the settings of the CFD simulation were consistent with those of the wind tunnel experiment, including the inflow reference wind speed (4.32 m/s) and geometric specifications. As illustrated in Fig. 3(b), a shallow street canyon (upwind building height= 32 m) and a deep street canyon (upwind building height= 57.6 m) with fixed street width (32 m) and building length (64 m) were chosen. The downwind building height stayed the same at 96 m. Additionally, a successfully-validated CFD model (conducted by Park et al.[24]) with the same turbulent model (RNG k-ε turbulence) as this work was introduced for comparison.

Fig. 3(c) shows the comparison among measurements and predicted distributions of normalized vertical wind speed (vertical wind speed/reference wind speed) and streamlines. Clearly, the experimental and numerical distributions of the normalized wind speed and streamlines were generally consistent for both shallow and deep street canyons. The incoming wind flowed over the roof of the upwind building and hit the windward surface of downwind building, creating a stagnation point on this surface as a result. Similar to the CFD simulation of Park et al.[24], the position of the stagnation point is well-predicted by the present CFD model. Below the stagnation point, there existed a strong downdraft in the vicinity of the windward surface of downwind building. As shown in Fig.3 (c), the current predicted maximum downdraft velocity is also close to that of the wind tunnel experiment and early CFD simulation. Then, this strong downdraft created a primary clockwise-rotating vortex within the street canyon. Generally, the present CFD model well-produced this primary vortex for both shallow and deep street canyons, although its intensity was marginally overestimated as compared to the wind tunnel experiment. Furthermore, this predicted stronger primary vortex suppressed the secondary recirculation zone in size and intensity, at the corner of the downwind building for both the shallow and deep street canyons. Possibly, when the thermal effect is considered, the forced convection will be slightly overestimated. As a result, the predicted average air temperature at the pedestrian level could be underestimated by the present CFD model marginally. Although, the present CFD model seems not be able to capture this kind of secondary recirculation near the downwind building, however, on the whole, it is reliable for the prediction of airflow within an asymmetric street canyon under the isothermal condition.

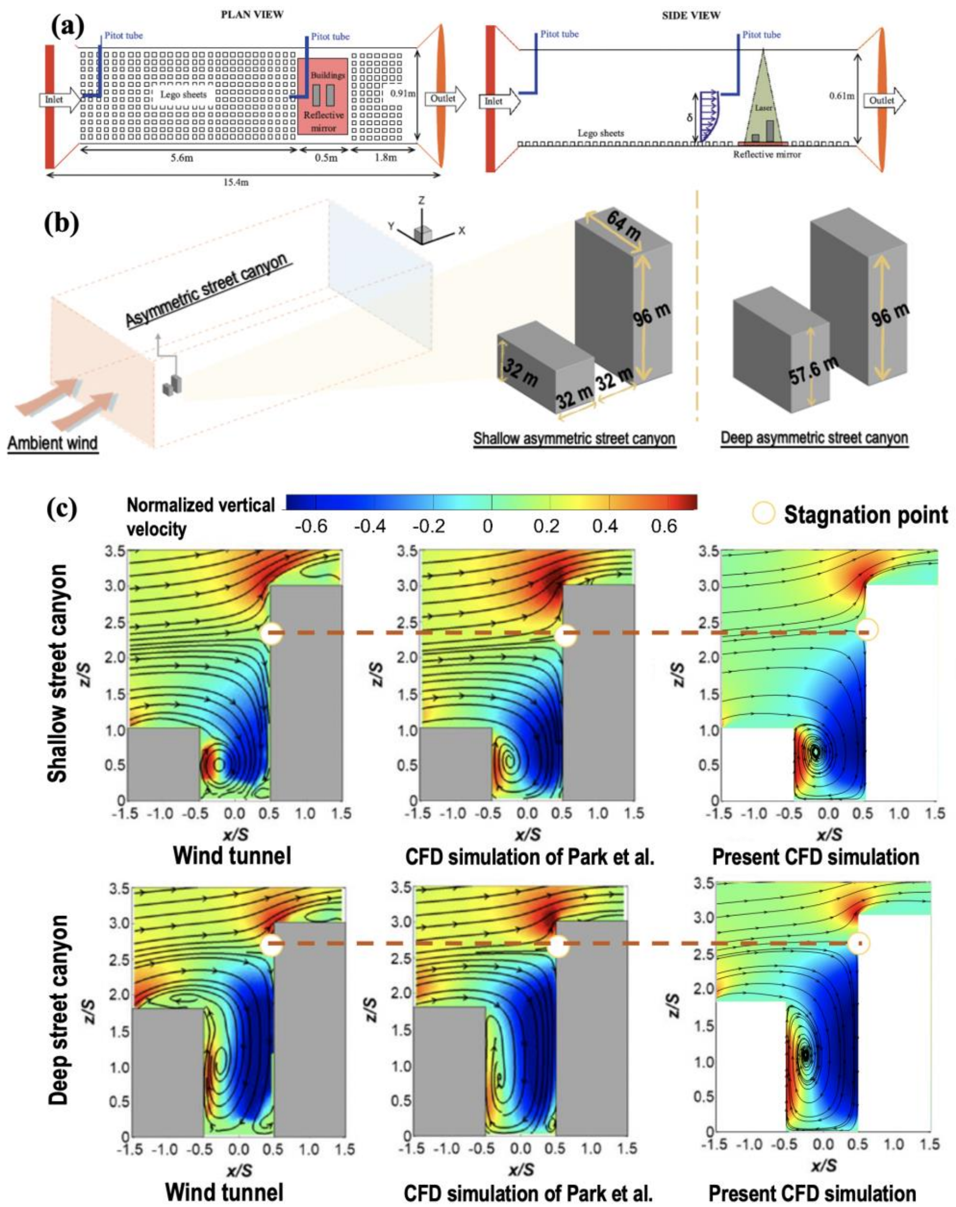

Fig.3 (a) An overview of the wind tunnel experiment by Addepalli and Pardyjak [26], (b) CFD model for the validation of isothermal airflow, and (c) Measured and predicted (by Park et al.[24] and present study) streamlines and normalized vertical wind components for the shallow and deep asymmetric street canyons.

3.1.2 Validation study of the thermal effect

Validation of in-canyon air temperature and wind speed in the wind tunnel experiment

For the validation of thermal effect, the measured in-canyon air temperature and wind speed in the previous wind tunnel experiment of Uehara et al. [56] were used.

Uehara et al. [56] investigated the influences of ground heating on airflow over an array of 3D buildings, with a group of simply shaped blocks (7 columns and 14 rows, as shown in Fig. 4 (b)). The characteristic length of each block is 0.1 m with an aspect ratio of 1 (height = width = length = 0.1 m). In the wind tunnel experiment, the floor was heated to a constant surface temperature T_g. The settings of the CFD simulation were consistent with those of the wind tunnel experiment, including the model geometry characteristics (Fig. 4 (b)) and bulk Richardson number (R_b, defined as $gH(T_{in}-T_g/\{(273.15+T_{in})(U_H)^2\})$ of −0.21 (unstable). Here, T_{in} is the ambient temperature and U_H is the mean wind speed at the building height H. The measured streamwise wind velocity and air temperature were obtained at the vertical section (z/H= 0-2) in the center of the street canyon between the fifth and sixth rows of the building arrays (Fig. 4 (b)).

Fig. 4 (c) illustrates a comparison of the simulated vertical profiles of normalized streamwise velocity u/U_{2H} (Fig. 4(c)) and normalized temperature $(T-T_g)/(T_{in}-T_g)$ with the experimental results from the wind tunnel tests. u and U_{2H} are the streamwise velocity and mean wind speed at the height of $2H$, respectively. It can be seen that the results of predicted streamwise flow velocities and air temperature agree well with the experimental data. Clearly, most of the deviations between the experimental data and the CFD results fall within nearly 5%. Besides, the simulated temperature profile near the ground is very close to the wind tunnel measurement, suggesting good agreement of the sharp temperature gradient near the ground. Also, the large velocity gradient at the roof level was well-predicted.

Generally, the current CFD modellings, including the numerical settings and turbulence model (RNG k-ε turbulence), are reliable in simulating the in-canyon air temperature and wind speed for the prediction of thermal effects.

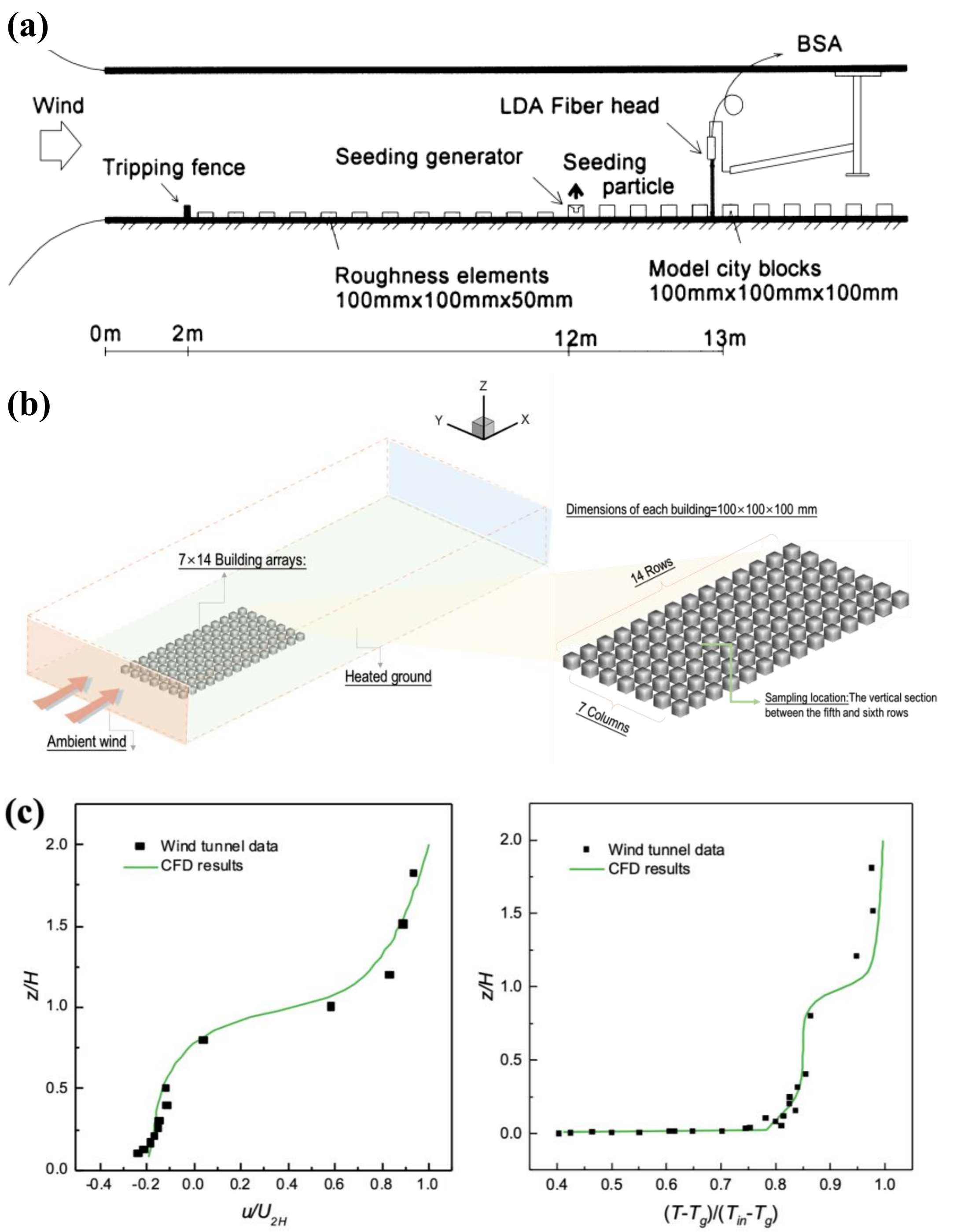

Fig.4 (a) An overview of wind tunnel experiment by Uehara et al. [56], (b) CFD model for the validation of air temperature and wind speed, and (c) Comparison of the simulated data with the wind tunnel data by Uehara et al. [56], in terms of normalized streamwise u/U_{2H} and normalized temperature $(T-T_g)/(T_{in}-T_g)$

Validation of wall temperature in field measurements

Additionally, to further evaluate the numerical accuracy of solar radiation prediction, the surface temperature data were compared with the field measurements that were obtained by Idczak et al. [57], who explored the thermal conditions inside a street canyon in an industrial area of Guerville, France (48°56' N, 1°44' E) on a sunny day (July 28). In the field experiment (Fig. 5(a)), the measurements were conducted in three parallel scaled street canyons that consisted of four empty steel containers covered by cement panels, with corresponding length of 18.3 m, height of 5.2 m, and width of 2.4 m. The width of the street was 2.1 m; therefore, the aspect ratio of the street canyon (defined as the ratio of the height of the building to the width of the street) is approximately 2.48. The street axis is oriented at an angle of 54° to the north. To evaluate the predicted thermal environment at 0800 LST and 1600 LST, the settings of the CFD simulation were consistent with those of the field measurement, including the physical model (Fig.5 (c)), the inlet air temperature (19.2 °C for 0800 LST and 28.3 °C for 1600 LST), wind speed (1.6 m/s for 0800 LST and 2.1 m/s for 1600 LST), and wind direction (south-west direction for both cases, almost parallel to the street axis). In the meanwhile, the CFD validation cases shared the same spectral optical and thermos-physical material properties of the container surface, including the specific heat (800 J/kg K), thermal conductivity (0.9 W/m K), and emissivity (0.95). The same coordinate (48°56' N, 1°44' E) and the time (July 28) of field measurements were input into the solar calculator of ANSYS Fluent to yield similar short-wave solar radiation for the validation case. Finally, the predictions of the wall temperature were compared with the field measurements in the southern façade of the second container at two levels (the average wall temperature along two sections, z/H = 0.21 and 0.84, as shown in Fig.5 (b)).

The predicted wall temperature is in satisfactory agreement with the recorded field measurement data (Table 3). At 0800 LST, the upper part of the southern façade was directly heated by solar radiation. In comparison, the lower part of the southern façade was still shaded by the downwind building. Accordingly, the field measurement data showed that there is a 3.5 °C higher wall temperature at z/H= 0.84 than at z/H = 0.21 (Table 3). This non-uniform distribution of wall temperature was also well-predicted by the present CFD model (wall temperature at z/H= 0.84 is 4.5 °C higher than that at z/H= 0.21). Similarly, at 1600 LST, the northern façade was directly heated by the solar radiation while the upwind building shaded the whole southern façade. Then, the air in the vicinity of northern façade became hotter, and this hotter air further heated the southern façade along with the in-canyon primary recirculation (from northern façade to southern façade near the ground). Accordingly, the field measurement results showed that the wall temperature at z/H= 0.21 was 0.3 °C higher than that at z/H= 0.87 (see Table 3). The present CFD model well-predicted this trend again (the wall temperature at z/H= 0.21 was 1.8 °C higher than that at z/H= 0.87). Generally, although there were still some differences between the predicted CFD results and field measurement data since the heat storage effects of the building walls were not considered, the prediction of the non-uniform wall temperature within the street canyon due to the realistic solar radiation was acceptable.

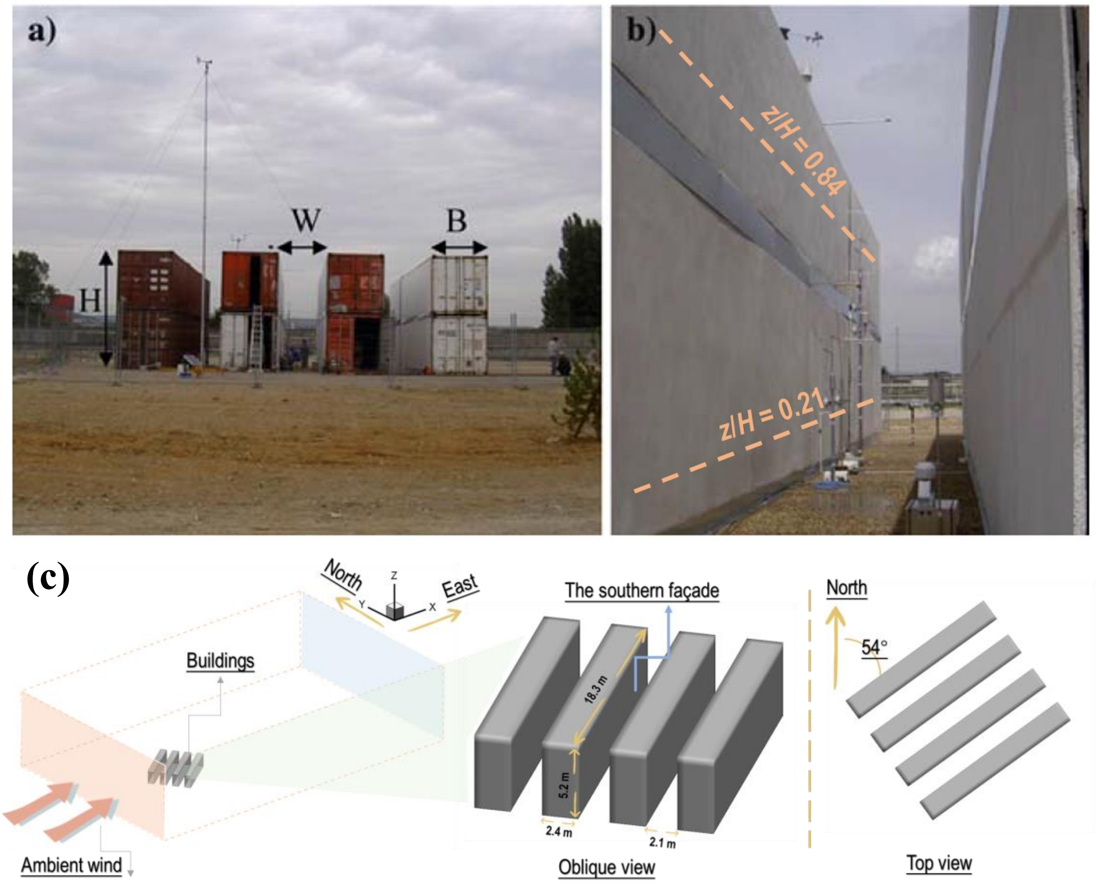

Fig. 5 Field measurements by Idczak et al.[57]: (a) An overview, (b) the instrumentation in the investigated street and (c) CFD model for the validation of wall temperature

Table 3 Comparison of the predicted non-uniform wall temperature with the field measurement data

Horizontal section	0800 LST (Background air temperature= 19.2 °C)		1600 LST (Background air temperature= 28.3°C)	
	CFD simulation	Field measurement	CFD simulation	Field measurement
$z/H = 0.21$	19.6 °C	21.4°C	30.1°C	29.2°C
$z/H = 0.84$	24.1°C	24.9°C	28.3°C	28.9°C

3.1.3 Validation study of pollutant dispersion

The current computational model for pollutant dispersion simulations was validated against the wind tunnel measurements conducted by Meroney et al. [58], who explored the street geometry effect on the dispersion of traffic pollutants within a 2D street canyon. Two wooden bars with height = width = 0.06 m and length =0.9m were mounted across the whole wind tunnel. The approaching wind direction was perpendicular to the canyon axis (Fig. 6 (a)). A ground-level pollutant line source (ethane, C_2H_6) parallel to the canyon axis was laid in the center of the canyon to represent traffic exhaust. Moreover, the pollutant was continually released at a steady rate of Q_e. The reference wind speed, U_{ref}, was recorded at a reference height of 0.65 m above the floor. To validate the predicted pollutant concentration, the settings of the CFD simulation were consistent with those of the wind tunnel experiment, as shown in Fig. 6 (b). The predictions of the normalized ethane concentration $C^* = CU_{ref}HL / Q_e$ were compared with the wind tunnel experiment data measured along the leeward and windward walls in the center vertical section of the canyon in Fig. 6 (a). Here, C is the volume fraction of ethane, and H and L are the height and the length of the buildings, respectively.

As demonstrated in Fig. 6 (c), on the windward side, the present CFD models slightly overestimate the pollutant concentration, while it slightly underpredicts the pollutant concentration in the lower part of the leeward side. Generally, the numerical settings and turbulence model are also suitable for predicting the pollutant dispersion with reasonable accuracy.

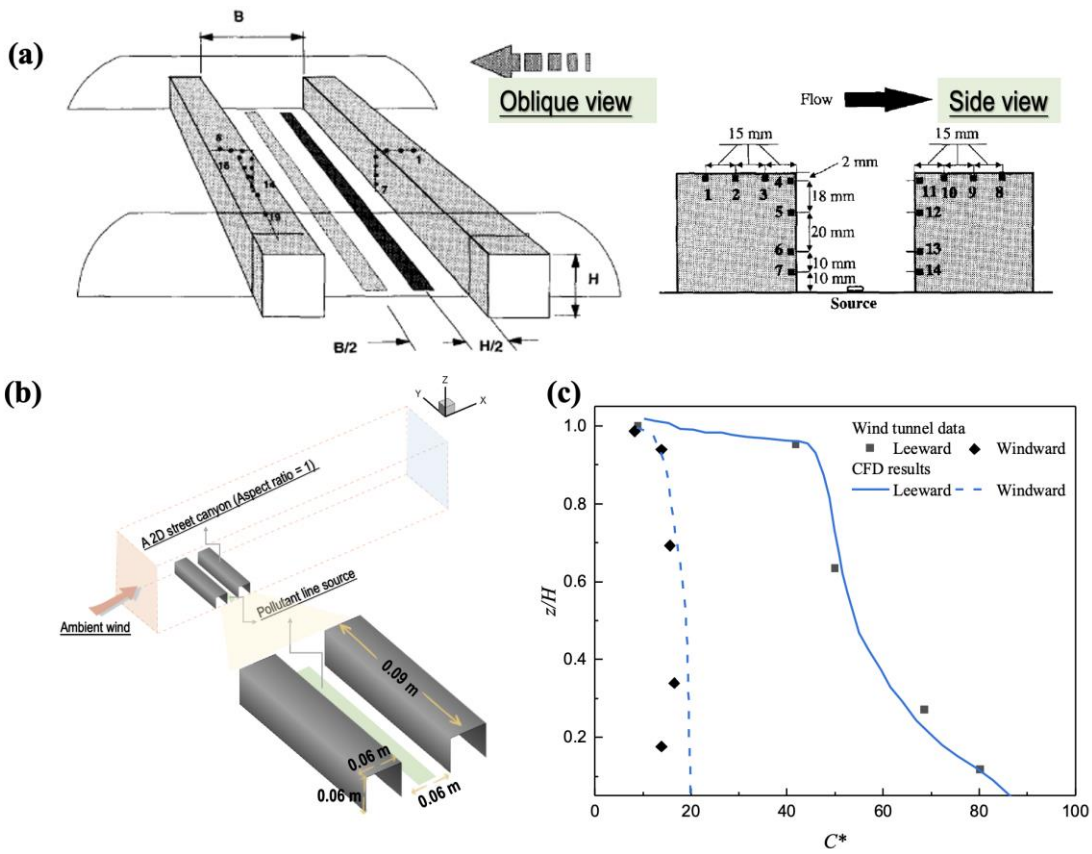

Fig. 6 (a) Schematic drawing of wind tunnel experiment by Meroney et al. [58], (b) CFD model for the validation of pollutant dispersion, and (c) Comparison of the simulated data with the wind tunnel data by Meroney et al. [58].

3.2 Effect of asymmetric configurations without solar radiation

To investigate the influence of solar radiation, the flow structures of asymmetric configurations were investigated without solar radiation as the baseline. According to Cui et al. [59], the flow structure did not change once the building Reynolds number Re_h (h = H_{max} =60 m) exceeded the critical value (Re_h = 3.4×10^4). In this study, the value of Re_h for low-wind-speed conditions is 1.88×10^6, which is far larger than the critical value of Re_h. Thus, the influence of the canyon configuration on the flow structure is similar for low and high wind speeds. Fig. 7 presents the wind velocity contours and 3D streamlines for the step-up and step-down street canyons, respectively, under a high wind speed. For the step-up street canyon, the flow structure changed only minimally with the increase of H_1, and the lower part of the street canyon was occupied by divergent flows that were caused by the strong downdraft flow (Fig. 7(c) and (d)). However, the wind velocity decreased slightly since the higher upstream building blocked the incoming flow and, therefore, attenuated the strength of the downdraft flow (Fig. 7 (a) and (b)). For the step-down street canyon with H_1/ H_2= 3/1, a large clockwise vortex occurred in the leeward region of the upstream building, and it also resulted in the formation of a downdraft flow and divergent flows in the lower space of the step-down street canyon (Fig. 7(g)). With the increase of H_2, the flow structure changed substantially. As shown in Fig. 7 (h), the downdraft flow disappeared, and the divergent flows were replaced by two elevated eddies. Moreover, the wind velocity changed minimally in the center of the street canyon, but it increased slightly near the lateral exit (Fig. 7 (e) and (f)).

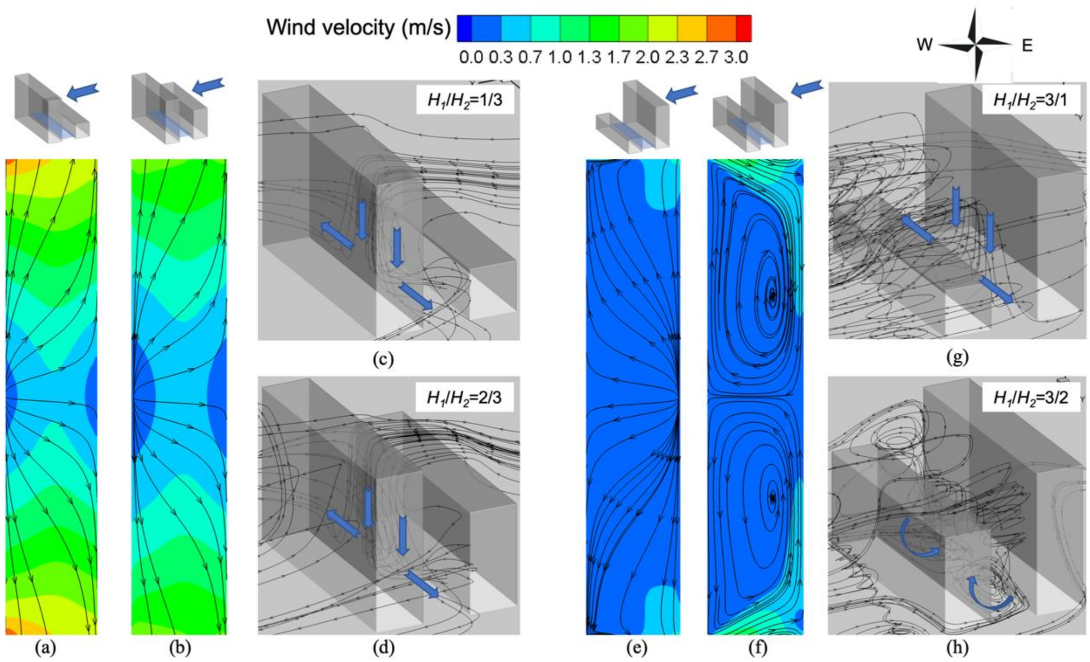

Fig. 7 Predicted wind velocity at the pedestrian level and 3D streamlines for various asymmetric street canyon configurations under a high wind speed without solar radiation: the wind velocity at the pedestrian level for (a) H_1/ H_2= 1/3, (b) H_1/ H_2= 2/3, (e) H_1/ H_2= 3/1, and (f) H_1/ H_2= 3/2; and 3D streamlines for (c) H_1/ H_2= 1/3, (d) H_1/ H_2= 2/3 (g) H_1/ H_2= 3/1, and (h) H_1/ H_2= 3/2. (The blue arrow denotes the flow direction within the street canyon.)

3.3 Effect of asymmetric configurations with solar radiation

Considering the solar radiation, Memon et al. [35] reported that the flow structure could differ significantly among incoming flow conditions. Thus, for the thermal flow, the influence of asymmetric configurations with solar radiation is analyzed at high wind speed (3 m/s, section 3.3.1) and low wind speed (0.5 m/s, Section 3.3.2). This thermal flow with solar radiation is dependent on the Reynolds number within our study range.

3.3.1 High incoming wind speed

Process I: To what height should the lower building be rebuilt?

Fig. 8 and Fig. 9 present the 3D streamlines and wind velocity contours under the high wind speed of 3 m/s for step-up and step-down street canyons, respectively. In the step-up street canyon, the buoyancy effect was relatively weak because the $|Ri|$ were low (1.27 to 4) (Table 4). The flow structure was still dominated by forced convection at 0800 LST (Fig. 8 (c) and (d)) and at 1600 LST (Fig. 8 (g) and (h)). The distributions of the 3D streamlines were similar to those in the cases without solar radiation (Fig. 7(c) and (d)), although the wind velocity decreased with the increase of H_1 (Fig. 8(a) and (b), and (e) and (f)). The average wind velocity at the pedestrian level decreased by approximately 0.4 m/s at 0800 and 1600 LST (as summarized in Fig. 12(a)). In the step-down street canyon, the forced convection still dominated the flow structure when H_1/H_2= 3/1 at 0800 LST (Fig. 9(c) with $|Ri|$ of 15.51) (Table 4). However, although the higher upwind building shaded the solar radiation into the street canyon at 0800 LST, the natural convection that was caused by solar radiation played a more critical role in the increase of H_2 ($|Ri|$ increased to 20.33 (Table 4)), thereby leading to the formation of an updraft flow (Fig. 9(d)), in contrast to the 3D streamlines without solar radiation (Fig. 7(d)). The possible explanation lies in the weak forced convection within this kind of street canyon. Once the airflow was heated by the windward surface entered the step-down canyon from the lateral shear layer (Fig.9 (d)), air flowed upwards because the natural convection is stronger than the weak forced convection. Furthermore, the lower part of the street canyon was occupied by convergent flows, and the wind velocity increased rapidly (Fig. 9(a) and (b)). The average wind velocity at the pedestrian level increased by 0.2 m/s (Fig. 12 (a)). At 1600 LST, the updraft flows were always observed (Fig. 9(g) and (h)) due to high $|Ri|$ (from 29.73 to 30.89) (Table 4)). When H_2 increased, $|Ri|$ decreased (a stronger shading effect on the downstream building led to weaker natural convection), and, thus, the wind velocity, which was affected by natural convection, decreased slightly (Fig. 9 (e) and (f)).

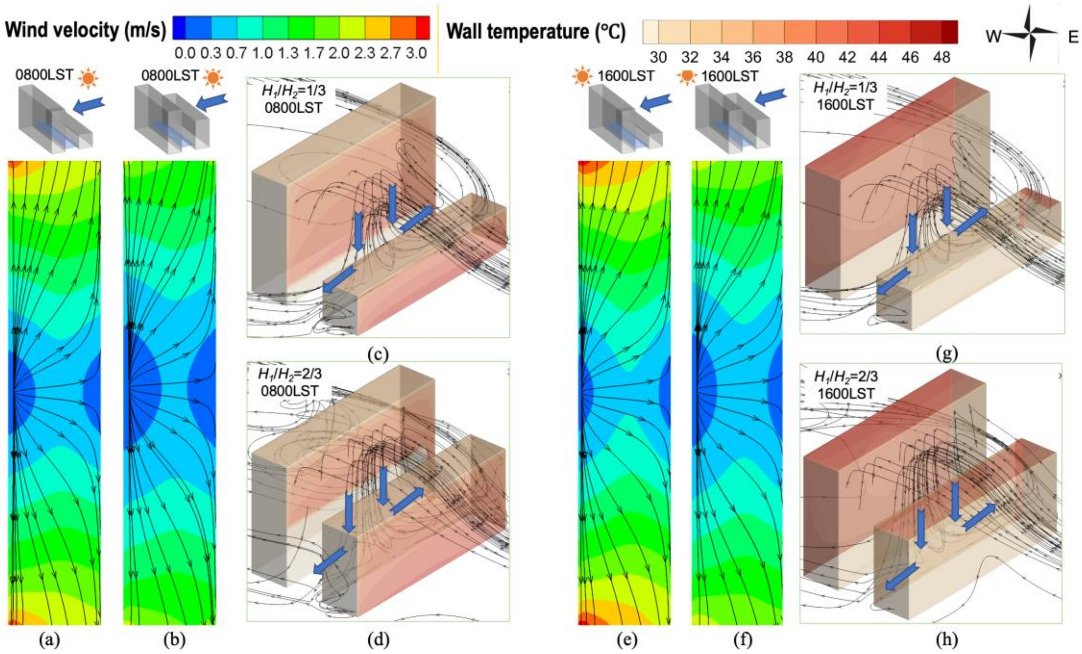

Fig. 8 Predicted wind velocity at the pedestrian level and 3D streamlines for various step-up street canyon configuration at LSTs of 0800 and 1600 under the high wind speed of 3 m/s: the wind velocity at the pedestrian level for (a) H_1/H_2= 1/3 at 0800 LST, (b) H_1/H_2= 2/3 at 0800 LST, (e) H_1/H_2= 1/3 at 1600 LST, and (f) H_1/H_2= 2/3 at 1600 LST; and 3D streamlines for (c) H_1/H_2= 1/3 at 0800 LST, (d) H_1/H_2= 2/3 at 0800 LST, (g) H_1/H_2= 1/3 at 1600 LST, and (h) H_1/H_2= 2/3 at 0800 LST. (The blue arrow denotes the flow direction within the street canyon.)

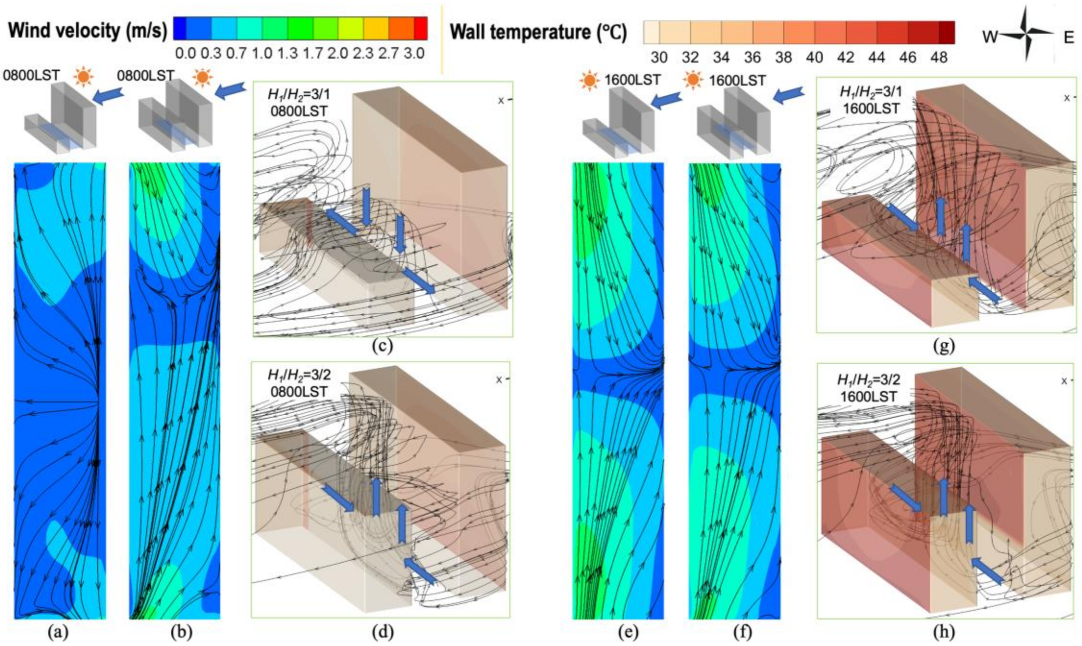

Fig. 9 Predicted wind velocity at the pedestrian level and 3D streamlines for various step-down street canyon configurations at LSTs of 0800 and 1600 under the high wind speed of 3 m/s: the wind velocity at the pedestrian level for (a) H_1/H_2= 3/1 at 0800 LST, (b) H_1/H_2= 3/2 at 0800 LST, (e) H_1/H_2= 3/1 at 1600 LST, and (f) H_1/H_2= 3/2 at 1600 LST; and 3D streamlines for (c) H_1/H_2= 3/1 at 0800 LST, (d) H_1/H_2= 3/2 at 0800 LST, (g) H_1/H_2= 3/1 at 1600 LST, and (h) H_1/H_2= 3/2 at 0800 LST. (The blue arrow denotes the flow direction within the street canyon.)

Table 4 Bulk Richardson numbers in the asymmetric street canyons under high wind speed

Case	Configuration	LST	$\|Ri\|$	Case	Configuration	LST	$\|Ri\|$
1	H_1/H_2= 1/3	0800	4.00	5	H_1/H_2= 3/1	0800	15.51
2		1600	1.27	6		1600	30.89
3	H_1/H_2= 2/3	0800	3.98	7	H_1/H_2= 3/2	0800	20.33
4		1600	2.38	8		1600	29.73

Fig.10 presents the distribution of the CO concentration under the high wind speed of 3 m/s. In the step-up street canyon, the concentration increased with the increase of H_1 due to the reduction of the wind velocity at 0800 (Fig. 10 (a) and (b)) and 1600 LST (Fig. 10 (c) and (d)). The average concentration increased by 48.8% at 0800 LST and by 39.0% at 1600 LST (see the summary in Fig. 12(b)). In the step-down street canyon, the divergent flows (Fig. 9(c)) transformed into convergent flows (Fig. 9(d)) near the ground at 0800 LST when H_2 increased. Therefore, more pollutants accumulated in the center of the street canyon, while the concentration near the lateral exit decreased (Fig. 10 (e) and (f)). At 0800 LST, the average concentration decreased by 8.2%(Fig. 12(b)). At 1600 LST, the concentration remained nearly unchanged (1.3%) due to only minor changes in the wind velocity (Fig. 9(g) and (h)).

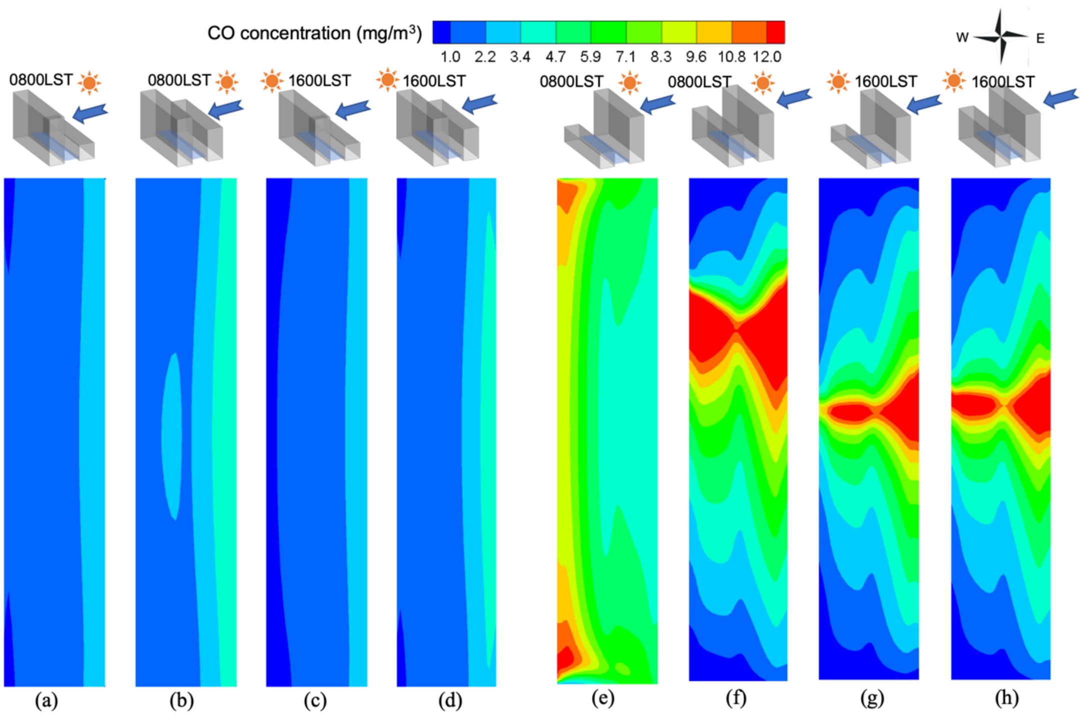

Fig. 10 Predicted CO concentrations at the pedestrian level for various asymmetric street canyon configurations at LSTs of 0800 and 1600 under the high wind speed of 3 m/s: the step-up canyon with (a) H_1/ H_2= 1/3 at 0800 LST, (b) H_1/ H_2= 2/3 at 0800 LST, (c) H_1/ H_2= 1/3 at 1600 LST, and (d) H_1/ H_2= 2/3 at 1600 LST; and the step-down canyon with (e) H_1/ H_2= 3/1 at 0800 LST, (f) H_1/ H_2= 3/2 at 0800 LST, (g) H_1/ H_2= 3/1 at 1600 LST, and (h) H_1/ H_2= 3/2 at 1600 LST.

Fig. 11 presents the contours of the air temperature under the high wind speed of 3 m/s. In the step-up street canyon, the air temperature at the pedestrian level was directly related to the temperature of the incoming flow because the relatively high wind velocity (up to 1.4 m/s) at the pedestrian level contributes to the dispersion of heat. Thus, the variation of the air temperature is small with an increase of H_1 (Fig.11 (a) and (b), (c) and (d)). In the step-down street canyon, the air temperature increased by 0.2-0.4 °C in the northern part of the street canyon (Fig.11 (e) and (f)), because the convergent flows were adverse to the heat dispersion at 0800 LST. The average air temperature increased slightly by 0.1°C (Fig. 12(c)). At 1600 LST, the air temperature decreased slightly due to the stronger shading effect that was provided by the high downstream building (Fig. 11(g) and (h)). The average air temperature decreased by 0.4°C (Fig. 12(c)).

In summary, the height increase of the lower building in the step-down canyon led to higher air quality and lower air temperature under high wind speed. However, the higher upstream building of the step-up canyon resulted in lower air quality but had only a minor influence on the thermal environment. When $|Ri| < 20$, the flow field was dominated by forced convection. The variation of $|Ri|$ slightly influenced air quality and air temperature. When $|Ri| > 20$, the flow field was dominated by natural convection. The increase of $|Ri|$ resulted in an increase of the air temperature and the decrease of the pollutant concentration at the pedestrian level.

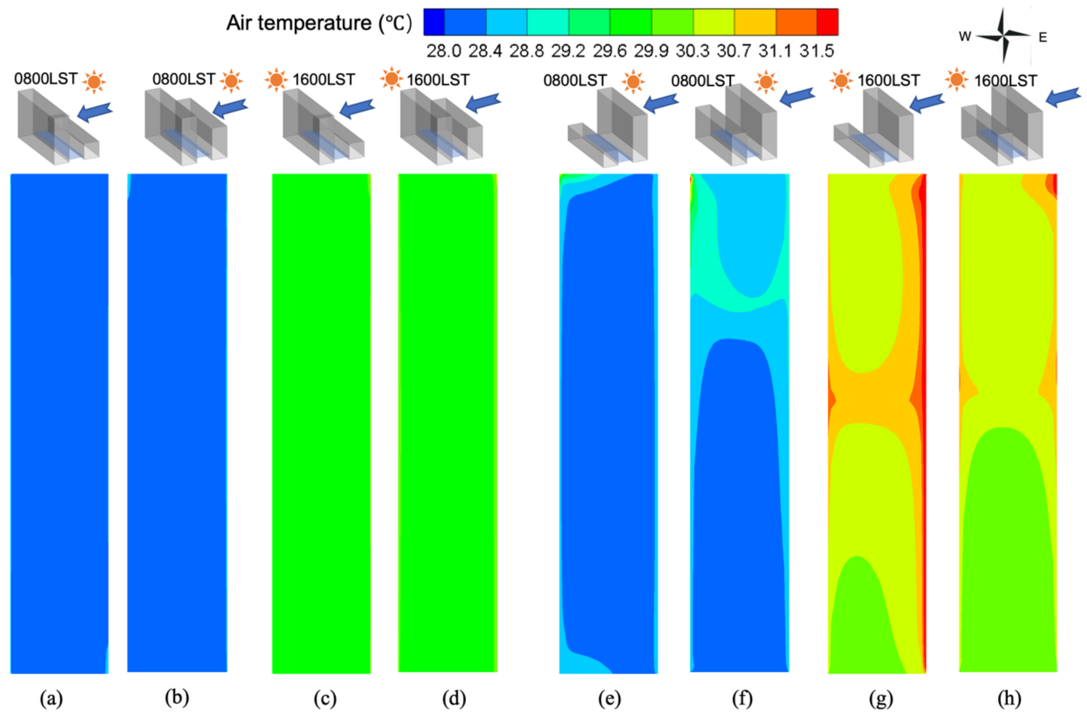

Fig. 11 Predicted air temperatures at the pedestrian level for various asymmetric street canyon configurations at LSTs of 0800 and 1600 under the high wind speed of 3 m/s: the step-up canyon with (a) H_1/H_2= 1/3 at 0800 LST, (b) H_1/H_2= 2/3 at 0800 LST, (c) H_1/H_2= 1/3 at 1600 LST, and (d) H_1/H_2=

2/3 at 1600 LST; and the step-down canyon with (e) H_1/H_2= 3/1 at 0800 LST, (f) H_1/H_2= 3/2 at 0800 LST, (g) H_1/H_2= 3/1 at 1600 LST, and (h) H_1/H_2= 3/2 at 1600 LST.

Process II: Which side of the street should be rebuilt?

To evaluate rebuilding process II, the average CO concentration and air temperature at the pedestrian level were compared between the step-up and the step-down street canyons in Fig. 12. For the step-up canyon with H_1/H_2= 1/3 and the step-down canyon with H_1/H_2= 3/1, the average CO concentration of the step-down canyon was 261.4% higher than that of the step-up canyon at 0800 LST (Fig. 12(b)), and the average air temperature of the step-down canyon was up to 1.1℃ (3.7%) higher than that of the step-up canyon at 1600 LST (Fig. 12(c)). For the step-up canyon with H_1/H_2= 2/3 and the step-down canyon with H_1/H_2= 3/2, lower air quality and higher air temperature were observed in the step-down canyon again. The average CO concentration of the step-down canyon (H_1/H_2= 3/2) was 123.1% higher than that of the step-up canyon (H_1/H_2= 2/3) at 0800 LST (Fig. 12(b)), and the average air temperature of the step-down canyon was up to 0.6℃ (2.0%) higher than that of the step-up canyon at 1600 LST (Fig. 12(c)). In summary, the step-down street canyon was outperformed by the step-up street canyon in both scenarios.

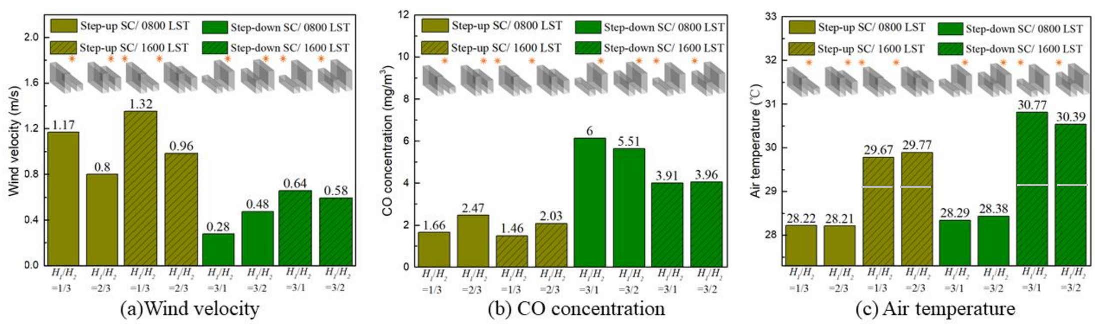

Fig. 12 Predicted average values at the pedestrian level for step-up and step-down cases: (a) the wind velocities, (b) CO concentration, and (c) Air temperature under the high wind speed of 3 m/s at LSTs of 0800 and 1600. The *y*-axis of Fig. 12 (c) starts from the reference air temperature (27.3 ℃) at 0800 LST, and the grey line denotes the reference air temperature (29.1℃) at 1600 LST.

3.3.2 Low incoming wind speed

Process I: To what height should the lower building be rebuilt?

Fig. 13 and Fig. 14 present the 3D streamlines and wind velocity contours under the low wind speed of 0.5 m/s. The natural convection had a significant influence on the flow structure. In the step-up street canyon, at 0800 LST, an updraft flow that was caused by the heated windward surface occurred in the street canyon with H_1/H_2= 1/3(Fig. 13(c)), which was opposite the high-wind case(Fig. 8(c)). The lower part was still occupied by divergent flows. With the increase of H_1, the natural convection strengthened ($|Ri|$ increased) (Table 5) and led to the formation of convergent flows (Fig. 13(d)). Thus, the average wind velocity at the pedestrian level increased by 0.3 m/s due to the convergent flows (see the summary in Fig. 17(a)). At 1600 LST, a downdraft flow was also observed in the street canyon with H_1/H_2= 1/3 (Fig. 13(g)) since the forced convection dominated the flow structure ($|Ri|$ = 7.50). With the increase of H_1, the downdraft flow still dominated within the canyon, but the natural convection strengthened ($|Ri|$ increased to 16.18). Thus, the average wind velocity at the pedestrian level decreased by 0.3 m/s (Fig. 17(a)) due to the reduction of the forced convection and the stronger natural convection. In the step-down street canyon, the flow structure was affected mainly by the stronger natural convection (higher $|Ri|$); therefore, updraft flows were observed (Fig. 14). At 0800 LST, the natural convection weakened (with relatively small $|Ri|$) due to lower wall temperature with the increase of H_2. Thus, the average wind velocity at the pedestrian level decreased slightly. Similarly, the average wind velocity decreased by 0.2 m/s at 1600 LST (Fig. 17(a)).

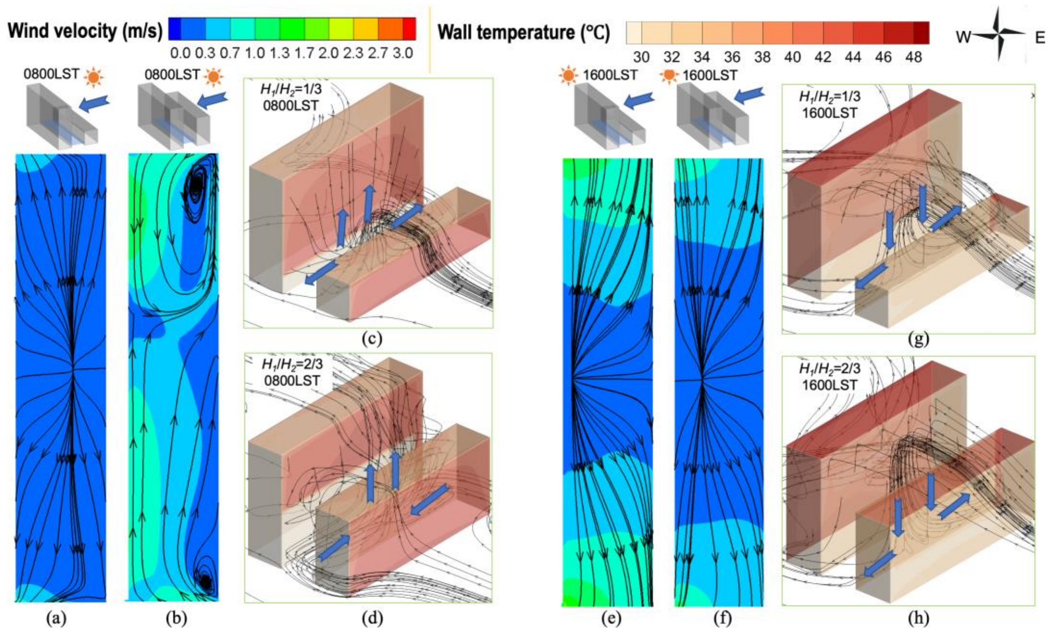

Fig. 13 Predicted wind velocity at the pedestrian level and 3D streamlines for various step-up street canyon configurations at LSTs of 0800 and 1600 under the low wind speed of 0.5 m/s: the wind velocity at the pedestrian level for (a) H_1/ H_2= 1/3 at 0800 LST, (b) H_1/ H_2= 2/3 at 0800 LST, (e) H_1/ H_2= 1/3 at 1600 LST, and (f) H_1/ H_2= 2/3 at 1600 LST; and 3D streamlines for (c) H_1/ H_2= 1/3 at 0800 LST, (d) H_1/ H_2= 2/3 at 0800 LST, (g) H_1/ H_2= 1/3 at 1600 LST, and (h) H_1/ H_2= 2/3 at 0800 LST. (The blue arrow denotes the flow direction within the street canyon.)

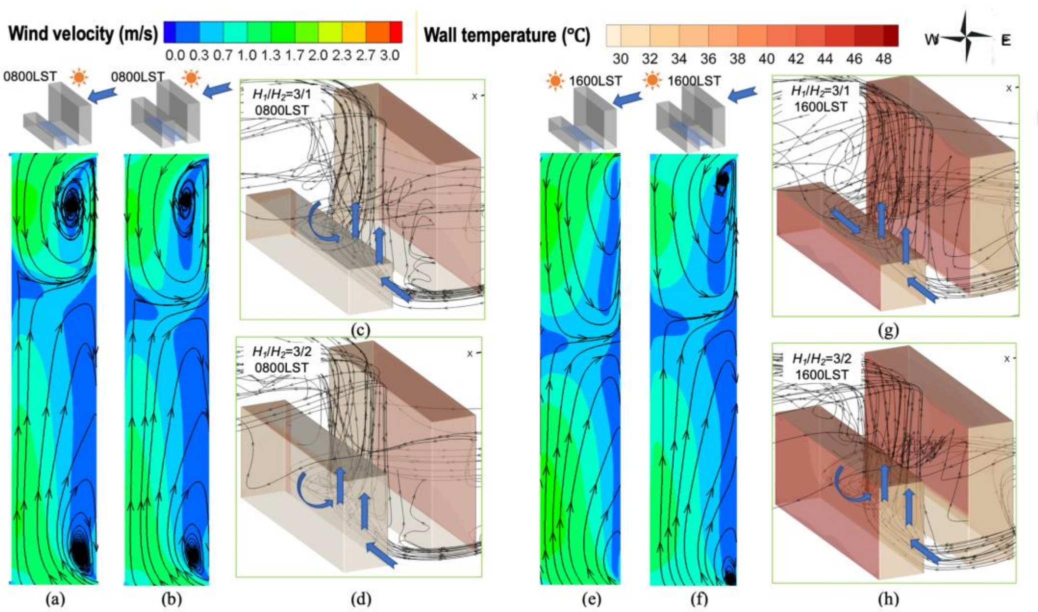

Fig. 14 Predicted wind velocity at the pedestrian level and 3D streamlines for various step-down street canyon configurations at LSTs of 0800 and 1600 under the low wind speed of 0.5 m/s: the wind velocity

at the pedestrian level for (a) H_1/ H_2= 3/1 at 0800 LST, (b) H_1/ H_2= 3/2 at 0800 LST, (e) H_1/ H_2= 3/1 at 1600 LST, and (f) H_1/ H_2= 3/2 at 1600 LST; and 3D streamlines for (c) H_1/ H_2= 3/1 at 0800 LST, (d) H_1/ H_2= 3/2 at 0800 LST, (g) H_1/ H_2= 3/1 at 1600 LST, and (h) H_1/ H_2= 3/2 at 0800 LST. (The blue arrow denotes the flow direction within street canyon.)

Table 5 Bulk Richardson numbers in the asymmetric street canyons under low wind speed

Case	Configuration	LST	$\|Ri\|$	Case	Configuration	LST	$\|Ri\|$
1	H_1/ H_2= 1/3	0800	25.16	5	H_1/ H_2= 3/1	0800	26.73
2		1600	7.50	6		1600	29.13
3	H_1/ H_2= 2/3	0800	26.01	7	H_1/ H_2= 3/2	0800	26.13
4		1600	15.67	8		1600	28.42

Fig. 15 presents the CO concentration contours under low wind speed. With the increase of H_1 at 0800 LST in the step-up street canyon, pollutants gathered in the northern part of the street canyon, but the concentrations in other areas decreased (Fig. 15 (a) and (b)) due to the variation of the flow structure. Thus, the average concentration decreased by 24.4% (Fig. 17 (b)). At 1600 LST, the average concentration increased by 77.1% due to a decrease in the wind velocity with the increase of H_1 (Fig. 17(b)). In the step-down street canyon, there is a minor increase of the concentration (3.4%), which is due to the similar wind velocity and flow structure at 0800 LST (Fig. 14(e) and (f)), while it increased by 46.9% due to the decrease of the wind velocity at 1600 LST (Fig. 17(b)).

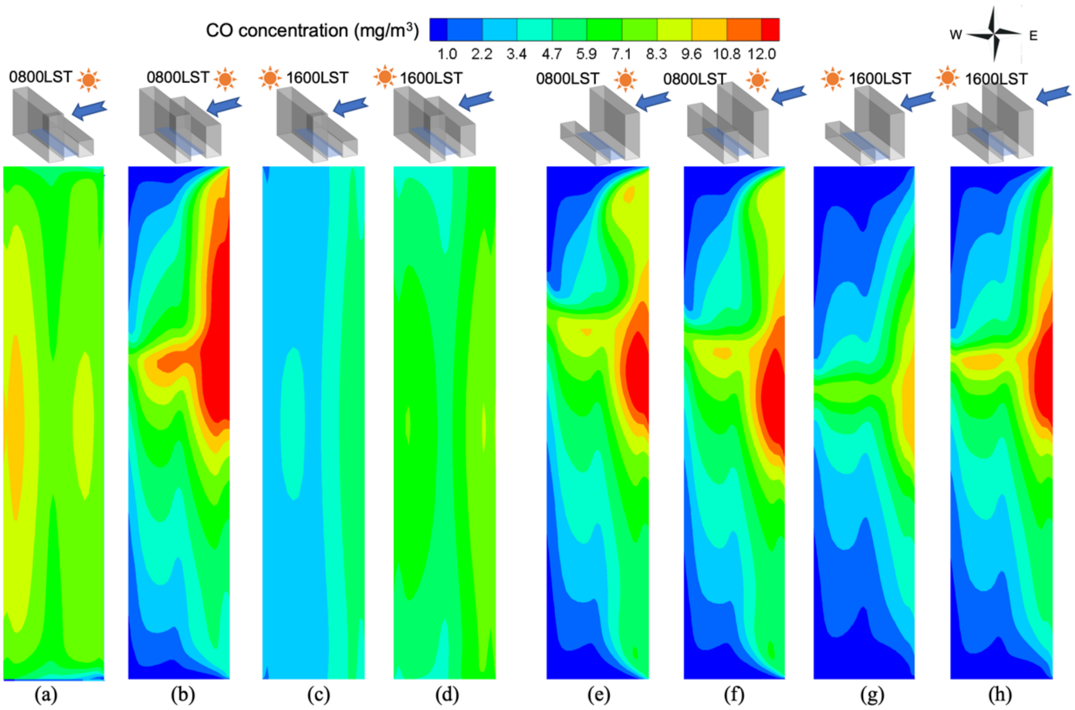

Fig. 15 Predicted CO concentrations at the pedestrian level for various asymmetric street canyon configurations at LSTs of 0800 and 1600 under low wind speed: the step-up canyon with (a) H_1/ H_2= 1/3 at 0800 LST, (b) H_1/ H_2= 2/3 at 0800 LST, (c) H_1/ H_2= 1/3 at 1600 LST, and (d) H_1/ H_2= 2/3 at 1600 LST; and the step-down canyon with (e) H_1/ H_2= 3/1 at 0800 LST, (f) H_1/ H_2= 3/2 at 0800 LST, (g) H_1/ H_2= 3/1 at 1600 LST, and (h) H_1/ H_2= 3/2 at 1600 LST.

Fig.16 presents the air temperature contours under low wind speed. In the step-up street canyon, the air temperature increased in the north but decreased in the south due to the convergent flow at 0800 LST (Fig. 16(a) and (b)). The average temperature changed slightly. At 1600 LST, the average temperature increased slightly, namely, by 0.3℃ (Fig. 17(c)), due to the reduction of the wind velocity. In the step-down street canyon, the average air temperature changed slightly at 0800 LST (Fig. 16(e) and (f)). This is because the higher upstream building almost blocked the solar radiation and the wind velocity also changed slightly. However, it decreased by 0.2℃ at 1600 LST due to the increase of the shading effect of the downstream building (Fig. 17(c)).

In summary, the height increase of the lower building resulted in the higher air quality at 0800 LST and lower air quality at 1600 LST in the step-up canyon under low wind speed; it resulted in lower air quality in the step-down canyon. The higher upstream building of the step-up canyon led to higher air temperature, while the higher downstream building of the step-down canyon resulted in lower air temperature. Similarly, the flow structure was dominated by forced convection when |*Ri*| < 20, and the variation of |*Ri*| was not directly related to air quality or air temperature. In contrast, when |*Ri*| > 20, the flow field was dominated by natural convection, and the increase of |*Ri*| also lead to an increase in the air temperature and a decrease in the pollutant concentration at the pedestrian level.

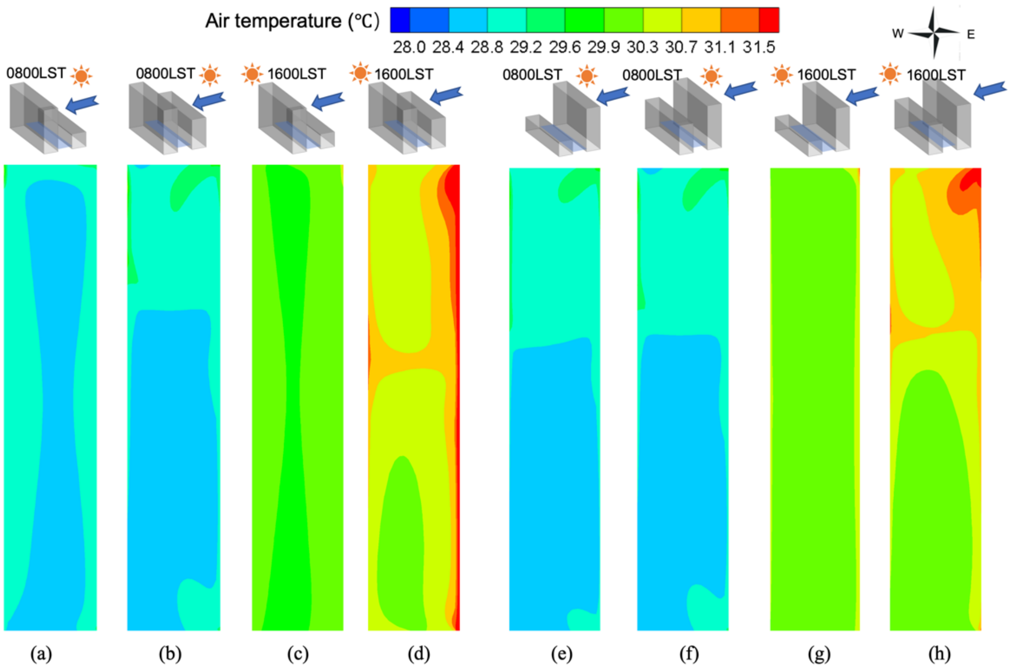

Fig. 16 Predicted air temperature at the pedestrian level for various asymmetric street canyon configurations at LSTs of 0800 and 1600 under low wind speed: the step-up canyon with (a) H_1/H_2= 1/3 at 0800 LST, (b) H_1/H_2= 2/3 at 0800 LST, (c) H_1/H_2= 1/3 at 1600 LST, and (d) H_1/H_2= 2/3 at 1600 LST; and the step-down canyon with (e) H_1/H_2= 3/1 at 0800 LST, (f) H_1/H_2= 3/2 at 0800 LST, (g) H_1/H_2= 3/1 at 1600 LST, and (h) H_1/H_2= 3/2 at 1600 LST.

Process II: On which side of the street should rebuilding be conducted?

The CO concentration and air temperature were further compared between the step-up and step-down street canyons in Fig. 17. For the step-up canyon (H_1/H_2= 1/3) and the step-down canyon (H_1/H_2= 3/1), divergent flows and convergent flows, respectively, occurred. Thus, higher CO concentration occurred in the center of the step-down canyon, but the concentration was substantially lower in other areas. The average concentration of the step-up canyon was 55.5% higher than that of the step-down canyon (Fig. 17 (b)) at 0800 LST. However, the average temperature of the step-down canyon was 0.6°C higher than that of the step-up canyon at 1600 LST(Fig. 17 (c)), due to a weak shading effect. For the step-up canyon (H_1/ H_2= 2/3) and the step-down canyon (H_1/ H_2= 3/2), the flow structures were similar, but the wind velocity of the step-up canyon was lower (Fig. 17 (a)). Thus, the average concentration of the step-up canyon was 38.1% higher than that of the step-down canyon at 1600 LST(Fig. 17(b)). The average air temperature of the step-down canyon was 0.3°C higher than that of the step-up canyon (Fig. 17(c)) at 1600 LST.

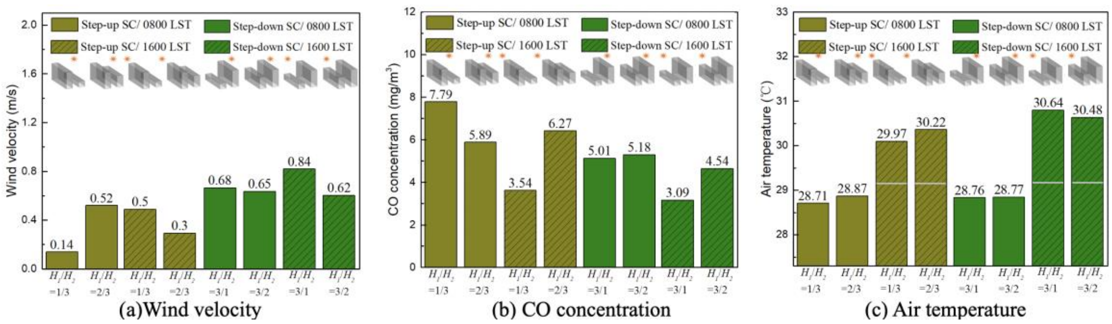

Fig. 17 Predicted average values at the pedestrian level: (a) the wind velocity, (b) the CO concentration and (c) the air temperature under low wind speed of 0.5 m/s at LSTs of 0800 and 1600. The *y*-axis starts from the reference air temperature (27.3 °C) at 0800 LST, and the grey line denotes the reference air temperature (29.1°C) at 1600 LST.

3.4 Multivariate regression (MLR) analysis

The relationships of the air temperature and air quality in the outdoor micro-environment with the key design factors (the upstream and downstream building heights H_1 and H_1, the canyon width W, and the reference wind speed U_{ref}) are generalized and summarized in this section. Multivariate regression analysis was conducted for 32 cases, which included eight configurations (H_1/H_2= 0.25, 0.33, 0.5, 0.67, 1.5, 2, 3, and 4), two reference wind speeds (0.5 and 3 m/s), and two local solar times (0800 and 1600 LST) in the city center of Hong Kong (latitude: 22°18' N, longitude: 114°10' E). The street orientation is in the north-south direction, and the ratio of building length to building width is kept constant at 5. Moreover, the prevailing wind is from the east for both 0800 LST and 1600 LST, and the background air temperature is 27.3 °C for 0800 LST and 29.1 °C for 1600 LST. Accordingly, four correlations were identified, as listed in Table 6. Four additional configurations (step-up canyons with H_1/H_2=1/4 and 2/4 and step-down canyons with H_1/H_2=4/1 and 4/2) were simulated to form a more sufficient database for more accurate analyses.

Table 6 Multivariate regression analysis for air temperature and CO concentration

Index	LST	Correlation	R^2
Air Temperature	0800	$T_{am}=30.301-0.317\frac{H_1}{W}-0.467\frac{H_2}{W}-0.145U_{ref}-0.02\frac{H_1}{W}U_{ref}-0.049\frac{H_2}{W}U_{ref}+0.103\frac{H_1}{W}\frac{H_2}{W}$	0.892
	1600	$T_{pm}=36.775-1.06\frac{H_1}{W}-2.086\frac{H_2}{W}-0.03U_{ref}-0.19\frac{H_1}{W}U_{ref}-0.062\frac{H_2}{W}U_{ref}+0.426\frac{H_1}{W}\frac{H_2}{W}$	0.835
CO Concentration	0800	$C_{am}=9.273-1.385\frac{H_1}{W}-0.269\frac{H_2}{W}-1.425U_{ref}+0.493\frac{H_1}{W}U_{ref}-0.32\frac{H_2}{W}U_{ref}+0.214\frac{H_1}{W}\frac{H_2}{W}$	0.802
	1600	$C_{pm}=1.437+0.771\frac{H_1}{W}+0.512\frac{H_2}{W}-0.122U_{ref}+0.125\frac{H_1}{W}U_{ref}-0.124\frac{H_2}{W}U_{ref}-0.052\frac{H_1}{W}\frac{H_2}{W}$	0.845

Improved thermal environment and air quality were identified through the correlations with multiple dimensionless parameters, which can serve as a reference for future asymmetric street canyon designs. Herein, the renewal planning of Shanghai Street in city centers of Hong Kong (Fig. 18 (a)) is considered as an example to preliminarily evaluate the variations of the outdoor thermal environment and air quality based on this multivariate regression analysis (Table 6).

In this case, because the ambient wind is from the east at an approximately 3 m/s speed and the street axis (North-south direction) is almost perpendicular to the ambient wind direction, the multivariate regression analysis conducted above is suitable for this urban renewal case, although the building length-width ratio ($L/W\approx$ 4) is slightly smaller. The width of Shanghai street is approximately 15.3 m, and the average heights of the upstream building and downstream building are approximately 74.9 m ($H_1/W\approx$

5) and 24.5 m (H_2/ $W \approx 2$), respectively. The downstream building will be rebuilt. Its new height will be 60 m (new H_2/ $W \approx 4$ and H_2/H_1 = 1.248 ≈ 5/4). According to the multivariate regression analysis, the average air temperature decreases by approximately 0.2ºC (am) and 0.4ºC (pm), and the average CO concentration decreases by approximately 10.4% (am) and 3.6% (pm). In summary, this renewal planning of windward buildings improves the outdoor thermal environment and air quality simultaneously.

To evaluate this assessment result, two step-down canyons with H_1/ H_2=5/2 and 5/4 with the same surrounding buildings were simulated via CFD, as shown in Fig. 18 (b). In Fig. 19, the air temperature and CO concentration decreased when H_2/ W increased from 2 to 4. The average air temperature at the pedestrian level decreased by 0.08ºC (0800 LST) and 0.42ºC (1600 LST), and the average CO concentration decreased by approximately 9.7% (0800 LST) and 4.8% (1600 LST). There is a large difference between the simulated values and MLR predictions. This is because the intricate surrounding buildings are not considered in the MLR analysis. However, MLR can well-predict the trend with the change in geometry of asymmetric street canyon. Generally, the multivariate regression analysis can evaluate the outdoor thermal environment and air quality beforehand for a north-south street canyon in the city centers of Hong Kong during the urban renewal process.

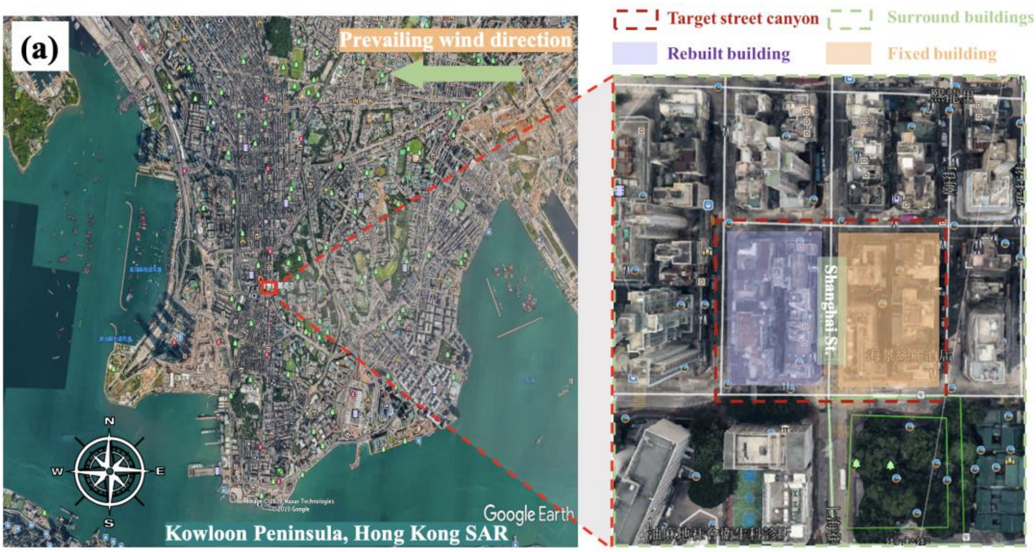

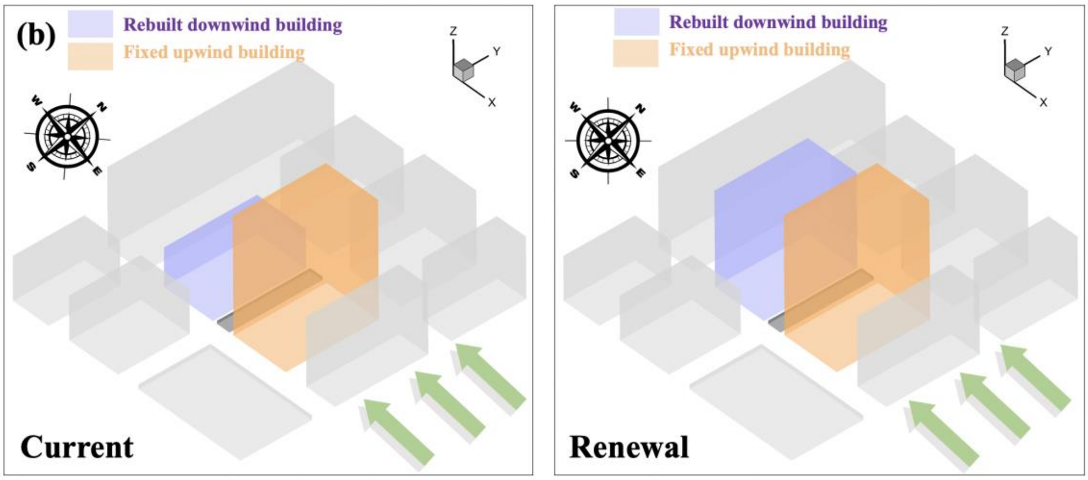

Fig.18 (a) Location and picture of the studied site. Source: Google Earth. (b) CFD models: the purple and orange blocks represent the rebuilt downwind building and the fixed upwind building, respectively, and the grey blocks represent the surrounding buildings around the target step-down street canyon.

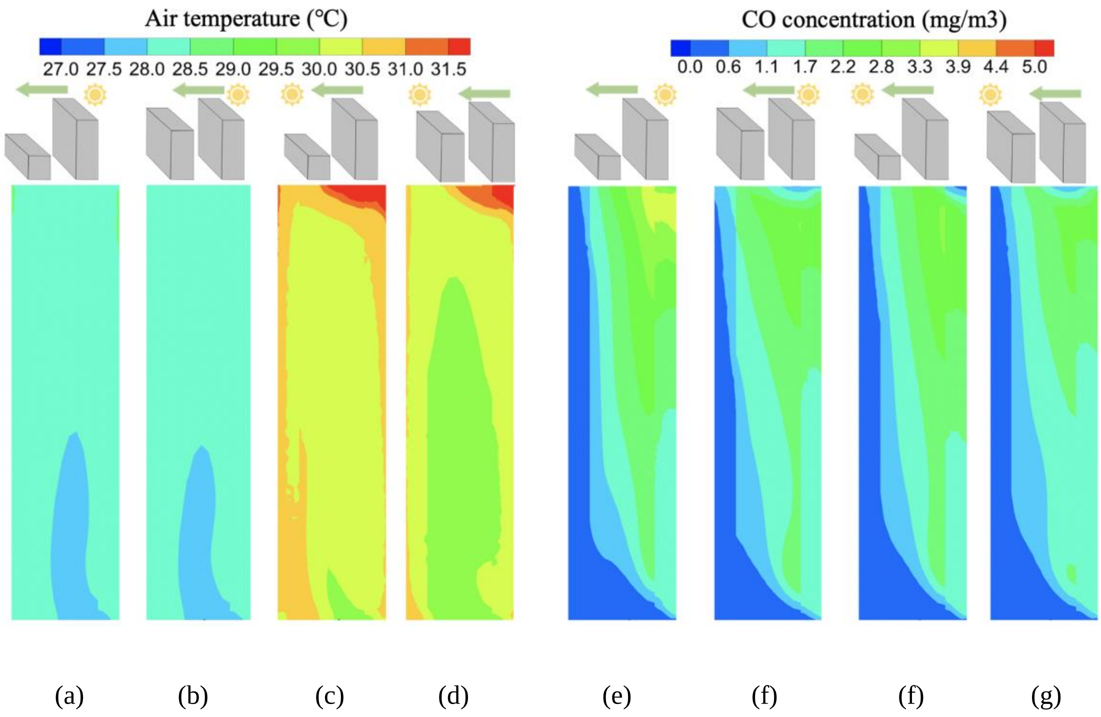

Fig. 19 Predicted air temperature and CO concentration at the pedestrian level: the air temperature for (a) H_1/ H_2= 5/2 at 0800 LST, (b) H_1/ H_2= 5/4 at 0800 LST, (c) H_1/ H_2= 5/2 at 1600 LST, and (d) H_1/ H_2= 5/4 at 1600 LST; and the CO concentration for (e) H_1/ H_2= 5/2 at 0800 LST, (f) H_1/ H_2= 5/4 at 0800 LST, (g) H_1/ H_2= 5/2 at 1600 LST, and (h) H_1/ H_2= 5/4 at 1600 LST.

4. Discussion and limitation

4.1 Discussion

In this section, some attained results of present studies will be compared with previous relevant studies in three aspects.

(i) Isothermal flow vs. thermal flow for asymmetric street canyon

Within a group of 3D isothermal step-up street canyons, Park et al. [24] found that the airflow undergoes development and mature stages with an increase in the building length-width ratio. According to Park et al. [24], the in-canyon flows for present models (both step-up and step down, with a building length-width ratio of $L/W > 2$) are at the mature stage. Without consideration of solar radiation, a primary vortex should be stable in position and induce strong outward flows in both spanwise directions. The present study shows that, under high wind speed, these strong outward flows and stable primary vortex features remain similar under isothermal and thermal conditions, as shown in Fig.7 and Fig. 8. Differently, under low wind speed, the heated windward surface of downwind building exhibited marked changes in the in-canyon flow, such as the disappearance of primary vortex (Fig. 13) and even the generation of strong inward flows in the deep step-up canyon ($H_1/H_2 = 2/3$, Fig. 13 (b)). Accordingly, the typical portal vortex in step-up canyons is virtually altered by this buoyancy effect under low wind speed.

(ii) 2D vs. 3D asymmetric street canyon

Xie et al. [27] pointed out that the heated windward surface of 2D step-up canyon leads to a higher in-canyon pollutant concentration in comparison with the heated leeward one. This is because the upward buoyancy flux opposes the downward advection flux along this windward surface. Interestingly, a similar phenomenon could be observed in the present 3D asymmetric street canyon by the same token. For instance, the windward side of the step-up canyon was heated at 0800 LST for present studies. Significantly, in Fig. 12, the average pollutant concentration at 0800 LST is 13.7 % - 21.7 % higher than that at 1600 LST under high wind speed. Also, under low wind speed, the heated windward side of the shallow step-up canyon at 0800 LST (H_1/H_2=1/3) even resulted in a nearly 120.0 % higher concentration than at 1600 LST (Fig. 17), whereas a slightly lower concentration (6.6%) was observed in a deep step-up canyon (H_1/H_2= 2/3). On the other hand, Xie et al. [27] also found that the heated leeward side of the step-down canyon caused higher concentration due to a decrease in the intensity of the vortex. Contrarily, in the present studies, the heated leeward side of the step-down canyon (1600 LST) led to a lower concentration (12.3% - 38.3%) than the heated windward side (0800 LST), under either high or low wind speed (Fig .12 and Fig .17). The reason is that the heated leeward side always caused a stronger convergent flow from the lateral exits, which can dilute the in-canyon pollutant concentration effectively. Comparatively, the 2D model were not be able to exhibit this kind of influence. In summary, similar conclusions are reached for both 2D and 3D step-up street canyons, while the inconsistent results are observed for the 2D and 3D step-down street canyons. The importance of three dimensional effects manifests.

(iii) The role of airflow in determining the thermal burden of asymmetric canyon

Rodríguez-Algeciras et al. [29] reported that a north-south street canyon with a higher west-side building could effectively reduce the thermal burden throughout the day due to its more substantial shading effect. In their study, they did not simulate the flow fields and consider the influence of different airflow caused by various asymmetric street canyons. However, a similar conclusion to the present study (with the consideration of the variations of airflow) is reached. In the current work, the step-up street canyon with the higher west-side building has lower air temperature than the step-down counterpart, under both high and low wind speeds. Accordingly, it can be concluded that the airflow plays a minor role in determining the thermal burden of the asymmetric canyon in comparison with the shading effect.

4.2 Limitations

The limitations of this study, which will be addressed in future work, are as follows:

(1) Steady computations were conducted in the current study. Thus, the temporal fluctuations in the wind velocity, direction, and diurnal temperature amplitude were not considered. Additionally, it has disregarded the heat storage effects of the building walls. The unsteady simulation can be included in future investigations to increase the prediction accuracy for practical urban environments.

(2) Because many previous studies focused on the outdoor environment of street canyons under a perpendicular wind direction, the prevailing ambient wind was introduced perpendicular to the street axis in the present simulation model. This is because perpendicular wind direction is usually related to the worst street canyon microclimate. However, the effect of wind direction and the impact of street direction should be explored in future work.

(3) Only was the thermal effect induced by solar radiation considered in this study. In effect, the anthropogenic heat (waste heat released into the atmosphere) also has a profound impact on the urban thermal effect and corresponds to the dilution potential of pollutants[60]. For instance, in the commercial district of Tokyo, Japan, Ohasai et al. [61] reported that the magnitude of waste heat flux from air-conditioners is over 1.5 times larger than the short wave flux caused by solar radiation on the building surface in summer. Similarly, in Houston, USA, Sailor and Lu [62] found the traffic-induced heat flux (heated traffic emission) in a major freeway is as high as 300 W/m^2, which is also of the order of sensible heat caused by solar radiation. For the present study, the windward surface of downwind building was shaded in 1600 LST, and the forced convection hence played a dominant role in determining the in-canyon flow structure. If this surface is heated by air-conditioners, marked changes of flow characteristic might be observed. Accordingly, to provide more comprehensive building design guidelines, these anthropogenic heat sources shall be considered in our future work.

(4) The street length is fixed for the present study. However, with the increase of street length, the interaction between the top shear layer and the lateral shear layer could be radically different, yielding distinct in-canyon flow features. Thus, the effect of street length-width ratio should be explored in future work.

(5) Whether the modelling set-up actually can be expected to yield in-city results, i.e., where the two buildings are densely surrounded by other high buildings, should be further verified in the future.

In spite of these existing limitations, the new findings here can improve the understanding of the thermal environment and air quality within the asymmetric street canyons. Also, this paper contributed to a CFD model to evaluate air temperature and pollutant concentration at the same time, with consideration of the buoyancy force for natural-convection flows and the realistic solar irradiance. It derived some correlations from multivariate regression to quickly evaluate the outdoor air quality and air temperature for the urban renewal processes.

5. Conclusions

This study investigated the influence of the asymmetric street canyon configuration on air temperature and air quality at the pedestrian level by considering realistic estimates of solar irradiation. Based on CFD calculations that were conducted using the ANSYS Fluent® software, we obtained two outdoor parameters: the air temperature and the CO concentration. The major results are summarized as follows:

(1) Without solar radiation, the variation of the height of the lower building led to a minor change in the flow structure in the step-up canyon but a significant change in the step-down canyon.

(2) With solar radiation, the increase of the height of the lower building of the step-up canyon led to an increase in the average CO concentration by 39% – 49% under high wind speed, and a decrease by 24% for 0800 LST and an increase by 77% for 1600 LST under low wind speed. In addition, the average air

temperature increased by 0.2℃ – 0.3℃ under low wind speed, while it was virtually unchanged under high wind speed. In contrast, when the height of the lower building of the step-down canyon increased, the average CO concentration increased by 47% for 1600 LST under low wind speed, while it was almost unchanged in the other three cases (<8%). In the meanwhile, the average air temperature reduced nearly 0.2℃ – 0.3 ℃ for 1600 LST under both high and low wind speed, while it essentially didn't change for the two 0800 LST cases.

(3) When $|Ri| < 20$, the flow field was dominated by forced convection, and the variation of Ri had an insignificant influence on air quality and air temperature. In contrast, when $|Ri| > 20$, the flow field was dominated by natural convection, and the increase of $|Ri|$ resulted in an increase in the air temperature and a decrease in the pollutant concentration.

(4) Under high wind speed, the thermal environment or air quality of the step-up canyon was always better than that of the step-down canyon; under low wind speed, the air quality was higher in the step-down canyon than in the step-up canyon, although the step-up canyon was still found to be cooler than the step-down canyon.

(5) A multivariate regression analysis for all of the simulated cases has been conducted with the following group of parameters: H_1/W, H_2/W and U_{ref}. Four correlations for the air temperature and CO concentration were identified. These correlations with multiple parameters provide a reference for the design of north-south asymmetric canyon configurations in the city centers of Hong Kong to simultaneously improve the thermal environment and air quality.

Reference:

[1] C. Peng, T. Ming, J. gui, Y. Tao, Z. Peng, Numerical analysis on the thermal environment of an old city district during urban renewal, Energy Build. 89 (2015) 18–31. https://doi.org/https://doi.org/10.1016/j.enbuild.2014.12.023.

[2] S.-J. Mei, J.-T. Hu, D. Liu, F.-Y. Zhao, Y. Li, H.-Q. Wang, Airborne pollutant dilution inside the deep street canyons subjecting to thermal buoyancy driven flows: Effects of representative urban skylines, Build. Environ. 149 (2019) 592–606. https://doi.org/https://doi.org/10.1016/j.buildenv.2018.12.050.

[3] A.-S. Yang, Y.-M. Su, C.-Y. Wen, Y.-H. Juan, W.-S. Wang, C.-H. Cheng, Estimation of wind power generation in dense urban area, Appl. Energy. 171 (2016) 213–230.

[4] A. Yang, C. Wen, C. Cheng, Y. Juan, CFD simulations to study the cooling effects of different greening modifications, Int J Env. Chem Ecol Geol Geophys Eng. 9 (2015) 808–814.

[5] W. Yang, N.H. Wong, C.-Q. Li, Effect of street design on outdoor thermal comfort in an urban street in Singapore, J. Urban Plan. Dev. 142 (2015) 5015003.

[6] I. Panagiotou, M.K.-A. Neophytou, D. Hamlyn, R.E. Britter, City breathability as quantified by the exchange velocity and its spatial variation in real inhomogeneous urban geometries: An example from central London urban area, Sci. Total Environ. 442 (2013) 466–477. https://doi.org/https://doi.org/10.1016/j.scitotenv.2012.09.001.

[7] J. Hang, Y. Li, M. Sandberg, R. Buccolieri, S. Di Sabatino, The influence of building height variability on pollutant dispersion and pedestrian ventilation in idealized high-rise urban areas, Build. Environ. 56 (2012) 346–360. https://doi.org/https://doi.org/10.1016/j.buildenv.2012.03.023.

[8] J. Liu, J. Niu, Q. Xia, Combining measured thermal parameters and simulated wind velocity to predict outdoor thermal comfort, Build. Environ. 105 (2016) 185–197. https://doi.org/https://doi.org/10.1016/j.buildenv.2016.05.038.

[9] C. Cai, T. Ming, W. Fang, R. de Richter, C. Peng, The effect of turbulence induced by different kinds of moving vehicles in street canyons, Sustain. Cities Soc. 54 (2020) 102015. https://doi.org/https://doi.org/10.1016/j.scs.2020.102015.

[10] C.-Y. Wen, Y.-H. Juan, A.-S. Yang, Enhancement of city breathability with half open spaces in ideal urban street canyons, Build. Environ. 112 (2017) 322–336. https://doi.org/https://doi.org/10.1016/j.buildenv.2016.11.048.

[11] W. Wang, E. Ng, Air ventilation assessment under unstable atmospheric stratification — A comparative study for Hong Kong, Build. Environ. 130 (2018) 1–13. https://doi.org/https://doi.org/10.1016/j.buildenv.2017.12.018.

[12] Y.-H. Juan, A.-S. Yang, C.-Y. Wen, Y.-T. Lee, P.-C. Wang, Optimization procedures for enhancement of city breathability using arcade design in a realistic high-rise urban area, Build. Environ. 121 (2017) 247–261. https://doi.org/https://doi.org/10.1016/j.buildenv.2017.05.035.

[13] A.-S. Yang, Y.-H. Juan, C.-Y. Wen, C.-J. Chang, Numerical simulation of cooling effect of vegetation enhancement in a subtropical urban park, Appl. Energy. 192 (2017) 178–200. https://doi.org/https://doi.org/10.1016/j.apenergy.2017.01.079.

[14] A.-S. Yang, C.-Y. Wen, Y.-H. Juan, Y.-M. Su, J.-H. Wu, Using the central ventilation shaft design within public buildings for natural aeration enhancement, Appl. Therm. Eng. 70 (2014) 219–230. https://doi.org/https://doi.org/10.1016/j.applthermaleng.2014.05.017.

[15] A.-S. Yang, Y.-H. Juan, C.-Y. Wen, Y.-M. Su, Y.-C. Wu, Investigation on wind environments of surrounding open spaces around a public building, J. Mech. 33 (2017) 101–113.

[16] L. Chen, E. Ng, X. An, C. Ren, M. Lee, U. Wang, Z. He, Sky view factor analysis of street canyons and its implications for daytime intra-urban air temperature differentials in high-rise, high-density urban areas of Hong Kong: a GIS-based simulation approach, Int. J. Climatol. 32 (2012) 121–136.

[17] Z.-L. Gu, Y.-W. Zhang, Y. Cheng, S.-C. Lee, Effect of uneven building layout on air flow and pollutant

dispersion in non-uniform street canyons, Build. Environ. 46 (2011) 2657–2665.
[18] X. Xiaomin, H. Zhen, W. Jiasong, The impact of urban street layout on local atmospheric environment, Build. Environ. 41 (2006) 1352–1363.
[19] F. Yang, K. Zhong, Y. Chen, Y. Kang, Simulations of the impacts of building height layout on air quality in natural-ventilated rooms around street canyons, Environ. Sci. Pollut. Res. 24 (2017) 23620–23635.
[20] C. Hao, X. Xie, Y. Huang, Z. Huang, Study on influence of viaduct and noise barriers on the particulate matter dispersion in street canyons by CFD modeling, Atmos. Pollut. Res. 10 (2019) 1723–1735.
[21] V.D. Assimakopoulos, H.M. ApSimon, N. Moussiopoulos, A numerical study of atmospheric pollutant dispersion in different two-dimensional street canyon configurations, Atmos. Environ. 37 (2003) 4037–4049.
[22] E.S.P. So, A.T.Y. Chan, A.Y.T. Wong, Large-eddy simulations of wind flow and pollutant dispersion in a street canyon, Atmos. Environ. 39 (2005) 3573–3582.
[23] Y. Miao, S. Liu, Y. Zheng, S. Wang, Y. Li, Numerical study of traffic pollutant dispersion within different street canyon configurations, Adv. Meteorol. 2014 (2014).
[24] S.-J. Park, J.-J. Kim, W. Choi, E.-R. Kim, C.-K. Song, E.R. Pardyjak, Flow Characteristics Around Step-Up Street Canyons with Various Building Aspect Ratios, Boundary-Layer Meteorol. 174 (2020) 411–431.
[25] B. Addepalli, E.R. Pardyjak, A study of flow fields in step-down street canyons, Environ. Fluid Mech. 15 (2015) 439–481.
[26] B. Addepalli, E.R. Pardyjak, Investigation of the flow structure in step-up street canyons—mean flow and turbulence statistics, Boundary-Layer Meteorol. 148 (2013) 133–155.
[27] X. Xie, Z. Huang, J. Wang, Z. Xie, The impact of solar radiation and street layout on pollutant dispersion in street canyon, Build. Environ. 40 (2005) 201–212.
[28] A. Qaid, D.R. Ossen, Effect of asymmetrical street aspect ratios on microclimates in hot, humid regions, Int. J. Biometeorol. 59 (2015) 657–677.
[29] J. Rodríguez-Algeciras, A. Tablada, A. Matzarakis, Effect of asymmetrical street canyons on pedestrian thermal comfort in warm-humid climate of Cuba, Theor. Appl. Climatol. 133 (2018) 663–679.
[30] N. Nazarian, J. Kleissl, CFD simulation of an idealized urban environment: thermal effects of geometrical characteristics and surface materials, Urban Clim. 12 (2015) 141–159.
[31] N. Nazarian, J. Kleissl, Realistic solar heating in urban areas: Air exchange and street-canyon ventilation, Build. Environ. 95 (2016) 75–93. https://doi.org/https://doi.org/10.1016/j.buildenv.2015.08.021.
[32] S. Bottillo, A.D.L. Vollaro, G. Galli, A. Vallati, Fluid dynamic and heat transfer parameters in an urban canyon, Sol. Energy. 99 (2014) 1–10. https://doi.org/https://doi.org/10.1016/j.solener.2013.10.031.
[33] S. Bottillo, A.D.L. Vollaro, G. Galli, A. Vallati, CFD modeling of the impact of solar radiation in a tridimensional urban canyon at different wind conditions, Sol. Energy. 102 (2014) 212–222. https://doi.org/https://doi.org/10.1016/j.solener.2014.01.029.
[34] Z. Li, H. Zhang, C.-Y. Wen, A.-S. Yang, Y.-H. Juan, Effects of frontal area density on outdoor thermal comfort and air quality, Build. Environ. 180 (2020) 107028. https://doi.org/https://doi.org/10.1016/j.buildenv.2020.107028.
[35] R.A. Memon, D.Y.C. Leung, C.-H. Liu, Effects of building aspect ratio and wind speed on air temperatures in urban-like street canyons, Build. Environ. 45 (2010) 176–188. https://doi.org/https://doi.org/10.1016/j.buildenv.2009.05.015.
[36] J.-J. Baik, J.-J. Kim, A numerical study of flow and pollutant dispersion characteristics in urban street canyons, J. Appl. Meteorol. 38 (1999) 1576–1589.

[37] HKO (Hong Kong Observatory), Statistical data of weather information in Hong Kong;, (2019).

[38] A. Aflaki, M. Mirnezhad, A. Ghaffarianhoseini, A. Ghaffarianhoseini, H. Omrany, Z.-H. Wang, H. Akbari, Urban heat island mitigation strategies: A state-of-the-art review on Kuala Lumpur, Singapore and Hong Kong, Cities. 62 (2017) 131–145.

[39] M. Schatzmann, B. Leitl, Issues with validation of urban flow and dispersion CFD models, J. Wind Eng. Ind. Aerodyn. 99 (2011) 169–186. https://doi.org/https://doi.org/10.1016/j.jweia.2011.01.005.

[40] Y. Tominaga, A. Mochida, R. Yoshie, H. Kataoka, T. Nozu, M. Yoshikawa, T. Shirasawa, AIJ guidelines for practical applications of CFD to pedestrian wind environment around buildings, J. Wind Eng. Ind. Aerodyn. 96 (2008) 1749–1761. https://doi.org/https://doi.org/10.1016/j.jweia.2008.02.058.

[41] P.J. Richards, R.P. Hoxey, Appropriate boundary conditions for computational wind engineering models using the k-ε turbulence model, in: Comput. Wind Eng. 1, Elsevier, 1993: pp. 145–153.

[42] B. Blocken, T. Stathopoulos, J. Carmeliet, CFD simulation of the atmospheric boundary layer: wall function problems, Atmos. Environ. 41 (2007) 238–252.

[43] Y. Qu, M. Milliez, L. Musson-Genon, B. Carissimo, Numerical study of the thermal effects of buildings on low-speed airflow taking into account 3D atmospheric radiation in urban canopy, J. Wind Eng. Ind. Aerodyn. 104–106 (2012) 474–483. https://doi.org/https://doi.org/10.1016/j.jweia.2012.03.008.

[44] S. Dugaria, M. Bortolato, D. Del Col, Modelling of a direct absorption solar receiver using carbon based nanofluids under concentrated solar radiation, Renew. Energy. 128 (2018) 495–508. https://doi.org/https://doi.org/10.1016/j.renene.2017.06.029.

[45] J.A. Palyvos, A survey of wind convection coefficient correlations for building envelope energy systems' modeling, Appl. Therm. Eng. 28 (2008) 801–808.

[46] A. Fluent, ANSYS fluent theory guide 15.0, Inc, Canonsburg, PA. (2013).

[47] Y. Tominaga, T. Stathopoulos, Turbulent Schmidt numbers for CFD analysis with various types of flowfield, Atmos. Environ. 41 (2007) 8091–8099. https://doi.org/https://doi.org/10.1016/j.atmosenv.2007.06.054.

[48] W.-Y. Ng, C.-K. Chau, A modeling investigation of the impact of street and building configurations on personal air pollutant exposure in isolated deep urban canyons, Sci. Total Environ. 468–469 (2014) 429–448. https://doi.org/https://doi.org/10.1016/j.scitotenv.2013.08.077.

[49] V. Yakhot, S.A. Orszag, Renormalization group analysis of turbulence. I. Basic theory, J. Sci. Comput. 1 (1986) 3–51. https://doi.org/10.1007/BF01061452.

[50] Z. Tan, J. Dong, Y. Xiao, J. Tu, A numerical study of diurnally varying surface temperature on flow patterns and pollutant dispersion in street canyons, Atmos. Environ. 104 (2015) 217–227. https://doi.org/https://doi.org/10.1016/j.atmosenv.2015.01.027.

[51] B.E. Launder, D.B. Spalding, The numerical computation of turbulent flows, in: Numer. Predict. Flow, Heat Transf. Turbul. Combust., Elsevier, 1983: pp. 96–116.

[52] T. Cebeci, P. Bradshaw, Momentum transfer in boundary layers, Hemi. (1977).

[53] K. An, S.-M. Wong, J.C.-H. Fung, E. Ng, Revisit of prevailing practice guidelines and investigation of topographical treatment techniques in CFD-Based air ventilation assessments, Build. Environ. 169 (2020) 106580. https://doi.org/https://doi.org/10.1016/j.buildenv.2019.106580.

[54] J. Hang, X. Chen, G. Chen, T. Chen, Y. Lin, Z. Luo, X. Zhang, Q. Wang, The influence of aspect ratios and wall heating conditions on flow and passive pollutant exposure in 2D typical street canyons, Build. Environ. (2019) 106536. https://doi.org/https://doi.org/10.1016/j.buildenv.2019.106536.

[55] A.W.M. Yazid, N.A.C. Sidik, S.M. Salim, K.M. Saqr, A review on the flow structure and pollutant

dispersion in urban street canyons for urban planning strategies, Simulation. 90 (2014) 892–916.

[56] K. Uehara, S. Murakami, S. Oikawa, S. Wakamatsu, Wind tunnel experiments on how thermal stratification affects flow in and above urban street canyons, Atmos. Environ. 34 (2000) 1553–1562. https://doi.org/https://doi.org/10.1016/S1352-2310(99)00410-0.

[57] M. Idczak, P. Mestayer, J.-M. Rosant, J.-F. Sini, M. Violleau, Micrometeorological Measurements in a Street Canyon during the Joint ATREUS-PICADA Experiment, Boundary-Layer Meteorol. 124 (2007) 25–41. https://doi.org/10.1007/s10546-006-9095-z.

[58] R.N. Meroney, M. Pavageau, S. Rafailidis, M. Schatzmann, Study of line source characteristics for 2-D physical modelling of pollutant dispersion in street canyons, J. Wind Eng. Ind. Aerodyn. 62 (1996) 37–56. https://doi.org/https://doi.org/10.1016/S0167-6105(96)00057-8.

[59] P.-Y. Cui, Z. Li, W.-Q. Tao, Numerical investigations on Re-independence for the turbulent flow and pollutant dispersion under the urban boundary layer with some experimental validations, Int. J. Heat Mass Transf. 106 (2017) 422–436.

[60] C. Yuan, A.S. Adelia, S. Mei, W. He, X.-X. Li, L. Norford, Mitigating intensity of urban heat island by better understanding on urban morphology and anthropogenic heat dispersion, Build. Environ. (2020) 106876.

[61] Y. Ohashi, Y. Genchi, H. Kondo, Y. Kikegawa, H. Yoshikado, Y. Hirano, Influence of air-conditioning waste heat on air temperature in Tokyo during summer: numerical experiments using an urban canopy model coupled with a building energy model, J. Appl. Meteorol. Climatol. 46 (2007) 66–81.

[62] D.J. Sailor, L. Lu, A top–down methodology for developing diurnal and seasonal anthropogenic heating profiles for urban areas, Atmos. Environ. 38 (2004) 2737–2748.

[63] D.K. Fidaros, C.A. Baxevanou, T. Bartzanas, C. Kittas, Numerical simulation of thermal behavior of a ventilated arc greenhouse during a solar day, Renew. Energy. 35 (2010) 1380–1386. https://doi.org/https://doi.org/10.1016/j.renene.2009.11.013.

Table A.1 Monthly means of prevailing wind direction at Hong Kong Observatory between 1981 -2010 (E denotes the east wind, and W denotes the west wind) [37]

Mouth	Jan.	Feb.	Mar.	Apr.	May.	Jun.	Jul.	Aug.	Sept.	Oct.	Nov.	Dec.	Avg.
Prevailing wind direction	E	E	E	E	E	E	W	E	E	E	E	E	E

Table A.2 Spectral optical and thermos-physical material properties[63]

Property	Fluid	Building	Ground
Materials	Air	Concrete	Asphalt
Density (kg/m^3)	1.225	2400	2360
Specific heat (J/kg K)	1006.43	750	920
Thermal conductivity (W/m K)	0.0242	1.7	0.75
Viscosity (kg/m S)	1.7894×10^{5}	-	-
Absorption coefficient (1/m)	0.19	0.9	0.9
Scattering coefficient (1/m)	0	0	-10
Refractive index	1	1.7	1.92
Emissivity, ε	0.9	0.7	0.95

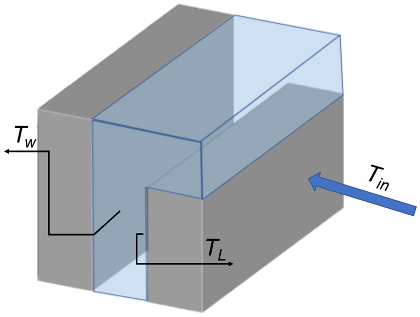

Fig. A.1 Schematic for the calculation of Richardson number (volume-average wind speed in the asymmetric canyons is calculated within the blue region)